Long-term OH variability of Miras

S. Etoka[1,2] **and A.M. Le Squeren**[3]

[1] Toruń Center for Astronomy, Nicolaus Copernicus University, PL-87100 Toruń, Poland
[2] Observatoire de Meudon, F-92195 Meudon Principal Cedex, France
[3] GRAAL Université de Montpellier II, F-34095 Montpellier Cedex, France

Abstract. We present here the results and interpretation of a long−term OH variability program conducted with the French Nançay Radiotelescope from 1980 to 1995. It concerns seven Mira stars: R Aql, RS Vir, S CrB, R LMi, RR Aql, U Her and UX Cyg. This study deals with the three OH maser lines observed in the Miras at 1612, 1665 and 1667 MHz. These OH variable stars have periods ranging from 290 to 580 days. The study presents the first insight of the long−term temporal behaviour of OH integrated flux variations as well as spectral component variations. The main aims are to determine the temporal behaviour of the OH maser emission and the longevity and variability of the spectral components. We find that the shapes of the OH curve are closer to the IR than the optical shapes and that the emissions at 1665 and 1667 MHz have a very similar behaviour while the emission at 1612 MHz behaves differently. The 1612 MHz emission shows smoother temporal variations and greater component longevity than the main line emission, leading to the conclusion that the 1612 MHz emission is coming from an outer part of the circumstellar shell and is more saturated than the main line emission. The study also shows the existence of inhomogeneities, especially differences between the front and back parts of the shell can be seen, and that OH variability curves undergo long term variations over several cycles.

Key words: masers — stars: circumstellar matter — stars: AGB and post-AGB; variables — ISM: molecules

1. Introduction

OH maser emission in late-type stars was first detected by Wilson & Barrett (1968). This emission comes from the circumstellar shell of these objects and can be detected in

Send offprint requests to: S. Etoka,
e-mail: setoka@jb.man.ac.uk/etoka@mesioq.obspm.fr

three of the four predicted transitions: in the 1612 MHz satellite line and in both main lines at 1665 and 1667 MHz. Miras are OH maser variable late-type stars, and can be observed at various other wavelengths, in the optical and infrared ranges. Harvey et al. (1974) and Fillit et al. (1977) have shown that the variations of the emissions in the visible, infrared and OH wavelengths are correlated. In particular, the proposition of infrared OH radiative pumping coming from dust was motivated by the correlation between the infrared and OH variations. Moreover, allowed transitions of the OH molecule exist in the near and far infrared.

The periods of the cyclic variations of these OH stars range from about 300 to 600 days (Kukarkin et al. 1969). Thus, one of the main constraints on studies of their variations is that several years of observations are needed.

The general shapes of the optical, infrared and OH variation curves are rather similar. Especially, one can see asymmetry between the ascending and descending parts of the curve corresponding to a difference between the rise time toward a maximum and the fall time toward a minimum (Le Bertre 1993; Herman & Habing 1985; van Langevelde et al. 1990, 1993).

For some of these stars, cyclic H_2O maser emission can also be observed. Gómez Balboa & Lépine (1986) have shown that some aperiodic variability can be observed in these H_2O maser emissions which span several cycles of the stellar periodicity. In some cases, they even observed superperiodic behaviour with a period equal to a multiple of the fundamental stellar period.

The standard OH spectrum of Miras is characterized by a two-peaked profile in which the peaks are sometimes called "blue" and "red" (i.e., respectively blue-shifted and red-shifted with respect to the stellar velocity). According to the standard model, i.e., an envelope in radial expansion (Reid et al. 1977), these emissions come from the front and back part of the shell respectively. Nevertheless, sometimes one can observe an

"intermediate" peak located between the two standard ones.

Except for eruptive Miras U Ori (Jewell et al. 1979, 1981; Cimerman 1979), X Oph (Etoka & Le Squeren 1996), R Leo, R Cnc, R LMi and U Her (Etoka & Le Squeren 1997), OH variability studies presented in the literature deal with only 2 or 3 consecutive cycles; variations over longer time spans have never been examined. The study presented here deals with observations in the 3 OH maser lines of 7 Miras performed over 15 years. These Miras are R Aql, RS Vir, S CrB, RR Aql, R LMi, U Her, and UX Cyg. The main aims of the study are to determine:

- the behaviour of the OH maser emission from one cycle to another;
- the longevity and variability behaviour of the various spectral components in each OH line;
- whether there are differences in the variations between standard and intermediate peaks.

In the next section we present the main characteristics of the observations. In Sect. 3 the methods of analysis used for this study are presented. In Sect. 4 the results concerning each star are presented separately. In Sect. 5 the main common characteristics of the various OH variations and their interpretation are given and, finally the conclusion of the study is given in Sect. 6.

2. Observations

The OH observations were made with the Nançay transit radio telescope which has a half beamwidth of $3.5'$ in α by $18'$ in δ at 18 cm wavelength. The system temperature was about 50 K. The ratio of flux to antenna temperature was 1.1 Jy K^{-1} at $0°$ declination. A frequency switching mode was used. Each observation lasted about one hour and achieved a mean rms of 0.03 Jy. The observations were made in both circular polarizations. Using a 1024 channel autocorrelation spectrometer, the first set of observations was obtained between February 1980 and December 1992 covering from 1 to 7 consecutive cycles depending on the star. During this period the autocorrelator was split into four banks of 256 velocity channels each, and the velocity resolution was about 0.14 km s^{-1} in the main lines and 0.145 km s^{-1} in the satellite line. Also, between February 1980 and March 1983 some linear polarization observations were also made for R Aql. For these observations the back end consisted of four banks of 64×6 kHz filters leading to a velocity resolution of about 1 km s^{-1}.

The second set of observations was obtained between January 1993 and January 1996, covering between one and two cycles depending on the star. For R LMi, the autocorrelator was split into four banks of 256 channels each leading to the same velocity resolution as previously mentioned. For the other sources, the autocorrelator was split into two banks of 512 channels each, thereby doubling the velocity resolution (i.e., $\simeq 0.07$ km s^{-1}).

According to observations made on the calibration source W12, antenna temperature values are estimated to be correct to $\pm 18\%$ between 1980 and 1984 and to $\pm 8\%$ for later observations. Thus, between 1980 and 1984, degrees of polarization lower than 0.1 should be taken with caution.

3. Method of analysis

The variability curves presented here deal with the integrated fluxes of the red, blue and intermediate peaks, when they exist, in each emitting OH maser line as well as the maximum intensity variations of the spectral components. These latter components were determined through a spectral decomposition by Gaussian fitting (Etoka 1996).

Observations of Miras at high velocity resolution, show that the spectral profile of these sources is not smooth, but is in fact composed of numerous rather narrow components blended together. Up to now, only the global integrated flux has been considered. According to a spectral decomposition method based on Gaussian fitting (Etoka 1996), we are able to study the OH variations in a more precise way. The accepted tolerance on the velocity divergence under which a component was considered to be the same from one fit to another was taken to be 1.5 times the poorest velocity resolution of the whole data set (i.e., 0.14 km s^{-1}). This leads to a tolerated divergence of 0.2 km s^{-1}.

Let us define the degree of circular polarization as follows:

$$[\text{RHC} - \text{LHC}]_{\text{freq.}} = \frac{\text{Flux}_{\text{RHC}} - \text{Flux}_{\text{LHC}}}{\text{Flux}_{\text{RHC}} + \text{Flux}_{\text{LHC}}} \tag{1}$$

where the flux can be the integrated or the maximum intensity flux depending on the case, and where "LHC" and "RHC" are respectively the left- and right-handed polarizations. The subscript "freq." refers to the frequency for which the degree of polarization has been calculated (i.e., 1612, 1665 or 1667 MHz).

For the calculation of the asymmetry factors we have used the curve fitting program developed by David et al. (1996) on the best sampled OH curve of integrated flux of each star over, when possible, 2 consecutive cycles.

4. Results

The 7 Miras presented here cover the infrared characteristics and period range of Miras. Table 1 presents these

Table 1. Main characteristics of the 7 selected Miras

Source	Period[1] days	type	$S^2_{12\mu m}$ Jy	$S^2_{25\mu m}$ Jy	$S^2_{60\mu m}$ Jy	$[25 - 12]$	$[60 - 25]$
R Aql	291	II	401.69	244.31	<139.49	−0.535	< −0.624
RS Vir	353	II	108.63	65.25	11.72	−0.540	−1.126
S CrB	360	I	200.68	125.52	19.00	−0.523	−1.200
R LMi	372	I	425.85	175.71	25.68	−0.703	−1.215
RR Aql	394	II	332.18	150.95	27.20	−0.661	−1.124
U Her	406	I	499.73	179.54	26.92	−0.763	−1.204
UX Cyg	561	II	171.55	101.39	43.60	−0.547	−0.747

1: Campbell L. 1985, *Studies of Long Period Variables.*
2: 1987 corrected IRAS flux.
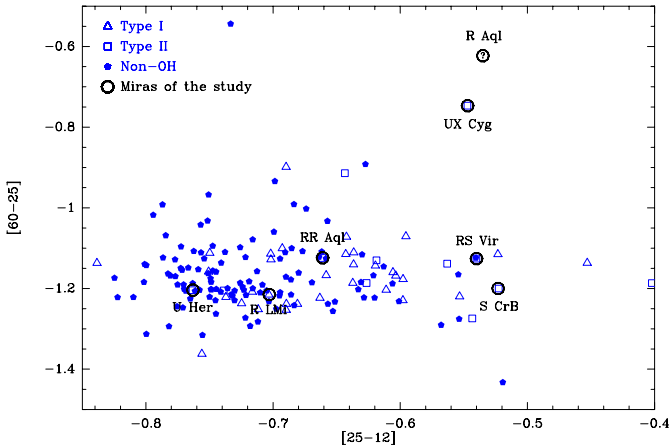
Fig. 1. Distribution of the 7 stars of the study in the color-color diagram of the nearby Miras (i.e., distant of less than 1 kpc from the Sun). The "?" is due to the incertainty concerning the 60 μm IRAS flux of R Aql and thus in its $[60 - 25]$ value

characteristics as follows: name of the source, mean period of the optical light curve, type of the maser emission, 12, 25 and 60 μm IRAS fluxes from Cols. 1 to 6 and finally in Cols. 7 and 8, the $[25 - 12]$ and $[60 - 25]$ color indexes calculated from the IRAS fluxes. Infrared fluxes are the 1987 corrected IRAS fluxes. Figure 1 shows the distribution of these stars in the color-color diagram of the nearest (distance < 1 kpc) Miras.

In this section the main characteristics of the OH variations are presented separately for each star. Corresponding optical light curves obtained from the AAVSO (*American Association of Variable Star Observers*) and the AFOEV (*Association Française des Observateurs d'Étoiles Variables*) are given with the OH variability curves for comparison.

For simplicity, we define the "amplitude of minimum−maximum variations" by $\Delta I_{\min-\max}$. This quantity is the relative difference in intensity or integrated flux which will be given in percent (i.e., $(I_{\max} - I_{\min}) \times 100\%/(I_{\max} + I_{\min})$), depending on the case, between a consecutive minimum and maximum in the variation curves. Moreover, we used the modified

Julian day defined as follows: Julian day −2400000 which will be called "Julian day".

4.1. R Aql

This star was observed in linear polarization between February 1980 and March 1983 and in circular polarization between March 1982 and March 1983 and from July 1993 to May 1995. For the linear polarization data set the four available banks were divided such that we observed both horizontal and vertical polarization only at 1667 MHz. Observations were performed in horizontal polarization at 1612 MHz while they were performed in vertical polarization at 1665 MHz. Because of the weakness of the 1665 MHz signal, observations in circular polarization were mainly performed at 1612 and 1667 MHz. Even though the velocity resolution of the linear polarization data is rather poor, the sampling is very good, with a separation between observations of 10 days to less than one month. The mean sampling in circular polarization is about 1 to 2 months.

4.1.1. Spectra

Figure 2 displays the spectra of this source in the 3 OH maser lines in both circular polarizations. The red and blue peaks are presented separately because of the great flux difference between them. One can see that the blue peak is wider than the red one for the 3 OH maser lines. The general spectral shapes at 1612 and 1667 MHz are roughly similar for the two peaks except for the intensity ratio between the red and blue peaks ($(\frac{I_{\rm red}}{I_{\rm blue}})_{1667} = 0.25$ and $(\frac{I_{\rm red}}{I_{\rm blue}})_{1612} = 20.0$ for the period presented in Fig. 2). However, the red part of the emission at 1612 MHz goes beyond the 1667 MHz emission by 1 km s^{-1}. On the other hand, the 1665 MHz profile is quite different from the two other profiles. Moreover, the 1665 MHz emission covers a smaller velocity range than the 1667 MHz emission. Indeed, both peaks at 1667 MHz go beyond those at 1665 MHz by more than 3 km s^{-1}.
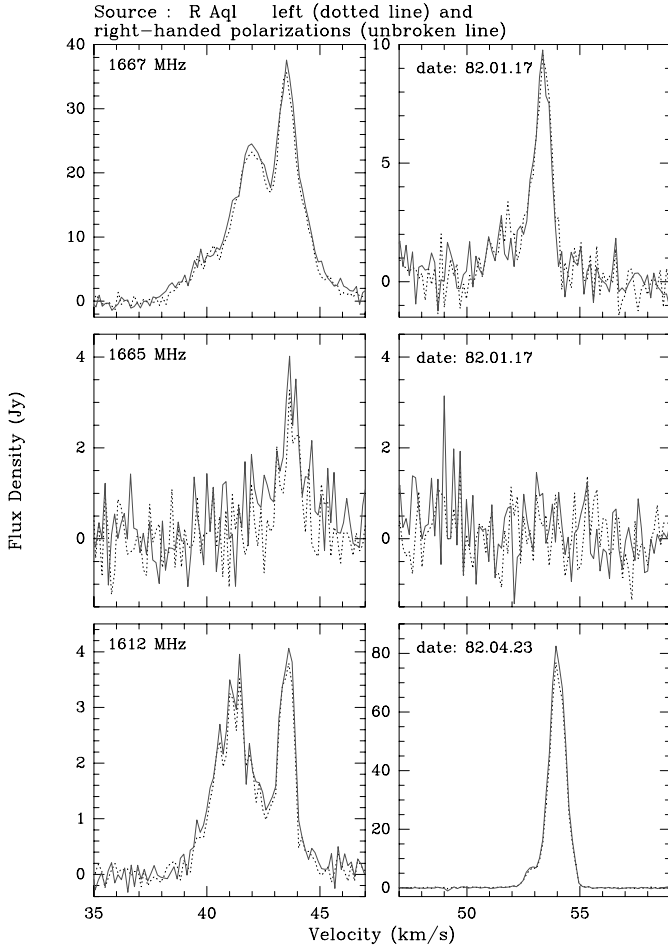
Fig. 2. Spectra of **R Aql** in the 3 OH maser lines in both circular polarizations. The red and blue peaks are displayed separately because of the great flux difference between them
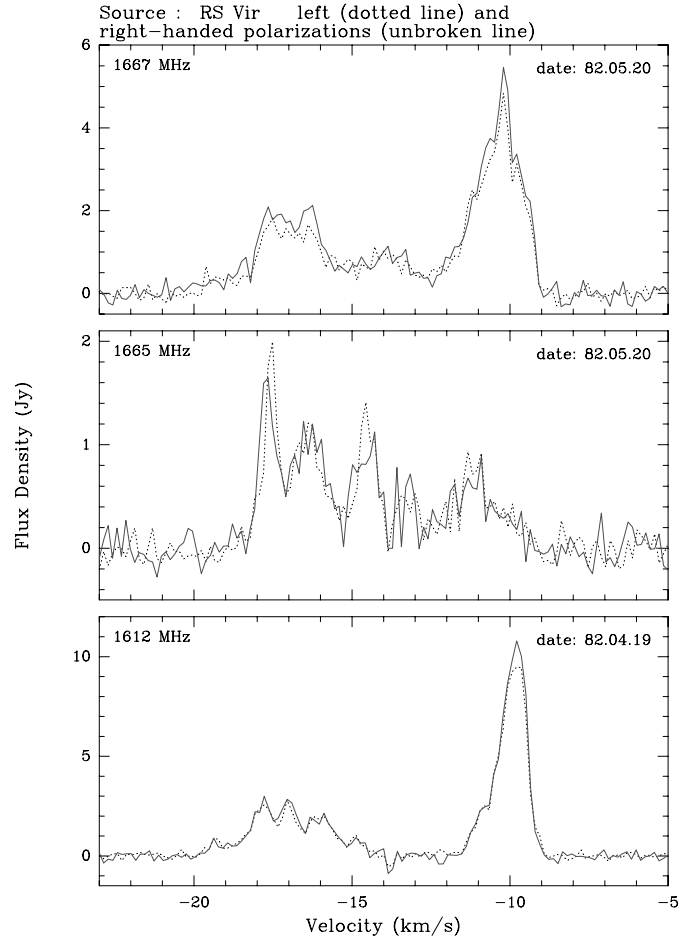

Fig. 3. Spectra of **RS Vir** in the 3 OH maser lines in both circular polarizations

4.1.2. Integrated flux

In Fig. 9 are presented the integrated flux variations of the red and blue peaks in linear and circular polarizations for the two epochs of observations.

The fitted curve of variations shows a delay of about 40–50 days with respect to the optical one (cf. Table 2). The general shape of the optical and OH variation curves is similar: a secondary maximum can be seen in both of them (cf. Figs. 9a,e).

This source is rather weakly circularly polarized at 1612 as well as at 1667 MHz ($-0.12 <[\mathrm{RHC-LHC}]_{1667} < 0.0$ and $-0.15 <[\mathrm{RHC-LHC}]_{1612} < 0.15$). Moreover, the degree of polarization is presumably not significant for the first set of data (i.e., between 1980 and 1983) because of expected calibration errors as previously mentioned in the Sect. 2.

The strongest line is clearly the satellite 1612 MHz line which can show integrated flux up to four times greater than the 1667 MHz line. The 1665 MHz flux is the faintest, often below the detection threshold.

Nevertheless, the largest $\Delta I_{\mathrm{min-max}}$ are reached for the 1665 and 1667 MHz integrated fluxes (cf. Table 4a). Moreover, we can clearly see from the first set of observations in linear polarization (i.e., from Figs. 9b to 9f) that the differences in $\Delta I_{\mathrm{min-max}}$ from one cycle to another at 1612 MHz are about the same while those differences are rather strong in the main lines.

Clearly, from one cycle to another the variations of the blue peak OH curve maxima are not correlated with the red one in any line (Figs. 9b-f). Nevertheless, variations at 1665 and 1667 MHz are similar for the same peak. This mimic behaviour between the 1665 and 1667 MHz OH variations may be explained by an overlap in the location of the maser emitting region in these two lines and shows moreover that the degree of non-saturation is comparable for both main lines. In contrast, the 1612 MHz variations are rather similar in both standard peaks and changes in the amplitude of variations from a cycle to another are very small. This confirms a higher level of saturation in this latter line in comparison to the main lines.

Table 2. Results of the OH curve fitting

Source	line[1] MHz	Pol.[2]	Peak[3]	Period[4] days	$f_{0\ \mathrm{OH}}^{4,5}$	$f_{0\ \mathrm{optical}}^{5}$	$t_{\mathrm{OH\ max}}^{4}$ days	$t_{\mathrm{optical\ max}}$ days	OH delay [6] days
R Aql	1612	H	R	285	0.57	0.43	44916	44872 ± 5	44 ± 10
RS Vir	1665	RHC	B	353	0.48	0.37	49333	49320 ± 15 [(*)]	13 ± 20
S CrB	1665	RHC	R	380	0.47	0.35	49327	49278 ± 5	49 ± 10
R LMi	1665	RHC	B	392	0.57	0.41	49638	49586 ± 10	52 ± 15
RR Aql	1665	LHC	B	394	0.56	0.31	49318	49249 ± 10	69 ± 15
U Her	1667	LHC	B	393	0.63	0.40	48330	48253 ± 5	77 ± 10
UX Cyg	1612	LHC	B	562	0.43	0.40	49617	49536 ± 5	81 ± 10

1: Line in which the curve fitting had been made.
2: Horizontal polarization (H), right- (RHC) and left-handed (LHC) polarizations.
3: Red (R) and blue (B) peaks.
4: Deduced from the OH curve fitting. The uncertainty for the calculated period and OH maximum date is of ± 5 days.
5: $f_0 = $ [rising time from a minimum toward a maximum]/period.
6: $t_{\mathrm{OH\ max}} - t_{\mathrm{optical\ max}}$.
∗: This value was obtained by superimposing 2 optical cycles for a better definition of the maximum.
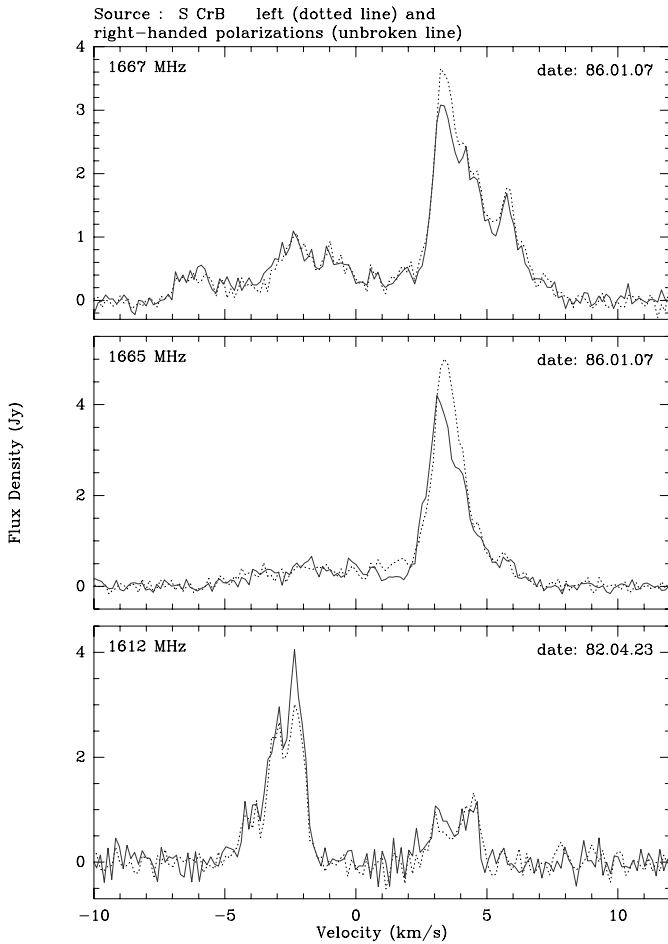
Fig. 4. Spectra of **S CrB** in the 3 OH maser lines in both circular polarizations
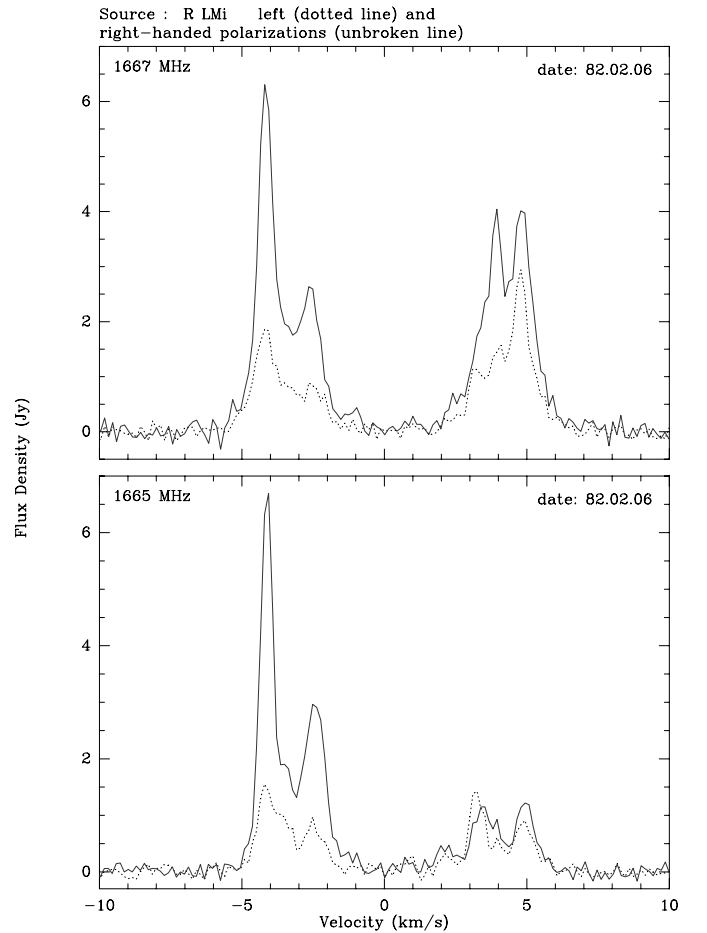
Fig. 5. Spectra of **R LMi** at 1665 and 1667 MHz in both circular polarizations

Table 3. Central velocity and full width at half-maximum (FWHM) of the fitted components which have shown a longevity greater than 1 stellar period of **R Aql** at 1612 and 1667 MHz for the 2 intervals of observations in circular polarization. For comparison are given too in the last column the velocity of the components determined by Herman & Habing at 1612 MHz (1985, i.e., column labelled H&H)

a_1) Red peak at 1612 MHz

	LHC km s^{-1}	FWHM km s^{-1}	RHC km s^{-1}	FWHM km s^{-1}	H&H km s^{-1}
interval 1[1]	$V_1 = 54.00$	0.814	$V_1 = 54.00$	0.810	54.04
	$V_2 = 52.91$	0.752	$V_2 = 52.92$	0.800	
interval 2[2]	$V_1 = 54.00$	0.843	$V_1 = 54.00$	0.835	
	$V_2 = 52.95$	0.849	$V_2 = 52.86$	0.700	

a_2) Blue peak at 1612 MHz

	LHC km s^{-1}	FWHM km s^{-1}	RHC km s^{-1}	FWHM km s^{-1}	H&H km s^{-1}
interval 1[1]	$V_1 = 43.54$	0.727	$V_1 = 43.53$	0.708	43.45
			$V_2 = 42.88$	0.504	
	$V_3 = 42.40$	0.420	$V_3 = 42.28$	0.475	
	$V_4 = 41.86$	0.334	$V_4 = 41.90$	0.336	
	$V_5 = 41.51$	0.404	$V_5 = 41.46$	0.372	
	$V_6 = 41.07$	0.402	$V_6 = 41.03$	0.345	41.01
	$V_7 = 40.58$	0.525	$V_7 = 40.55$	0.370	
	$V_8 = 39.98$	0.529	$V_8 = 40.11$	0.480	
interval 2[2]	$V_1 = 43.54$	0.733	$V_1 = 43.54$	0.689	
	$V_2 = 42.85$	0.423	$V_2 = 42.84$	0.463	
	$V_3 = 42.37$	0.341	$V_3 = 42.36$	0.327	
	$V_4 = 41.92$	0.385	$V_4 = 41.93$	0.353	
	$V_5 = 41.47$	0.333	$V_5 = 41.50$	0.340	
	$V_6 = 41.04$	0.393	$V_6 = 41.05$	0.408	
	$V_7 = 40.61$	0.390	$V_7 = 40.60$	0.440	
	$V_8 = 40.19$	0.468	$V_8 = 40.13$	0.451	
	$V_9 = 39.58$	0.510	$V_9 = 39.53$	0.558	

b_1) Red peak at 1667 MHz

	LHC km s^{-1}	FWHM km s^{-1}	RHC km s^{-1}	FWHM km s^{-1}
interval 1[1]	$V_1 = 53.48$	0.683	$V_1 = 53.47$	0.706
	$V_2 = 52.82$	0.603	$V_2 = 52.89$	0.616
	$V_3 = 52.46$	0.452	$V_3 = 52.44$	0.633
	$V_4 = 51.82$	0.652	$V_4 = 51.77$	0.565
interval 2[2]	$V_1 = 53.43$	0.762	$V_1 = 53.47$	0.731
	$V_2 = 52.69$	0.587	$V_2 = 52.59$	0.511
	$V_3 = 51.78$	0.573	$V_3 = 52.01$	0.524
			$V_4 = 50.91$	0.813

b_2) Blue peak at 1667 MHz

	LHC km s^{-1}	FWHM km s^{-1}	RHC km s^{-1}	FWHM km s^{-1}
interval 1[1]			$V_1 = 44.98$	0.465
	$V_2 = 44.45$	0.569	$V_2 = 44.39$	0.485
	$V_3 = 43.55$	0.819	$V_3 = 43.56$	0.896
	$V_4 = 42.52$	0.654	$V_4 = 42.57$	0.637
	$V_5 = 41.84$	0.681	$V_5 = 41.87$	0.587
	$V_6 = 41.17$	0.760	$V_6 = 41.20$	0.590
	$V_7 = 40.13$	0.654		
interval 2[2]			$V_1 = 45.31$	0.647
	$V_2 = 44.41$	0.489	$V_2 = 44.40$	0.516
	$V_3 = 43.44$	0.942	$V_3 = 43.54$	0.839
			$V_4 = 42.80$	0.507
	$V_5 = 42.40$	0.540	$V_5 = 42.29$	0.453
	$V_6 = 41.85$	0.544	$V_6 = 41.83$	0.572
	$V_7 = 41.33$	0.509	$V_7 = 41.24$	0.474
	$V_8 = 40.76$	0.798	$V_8 = 40.79$	0.608

1: Interval of Julian days [45000 − 45400]. 2: Interval of Julian days [49150 − 49850].

Source : RR Aql   left (dotted line) and
right-handed polarizations (unbroken line)
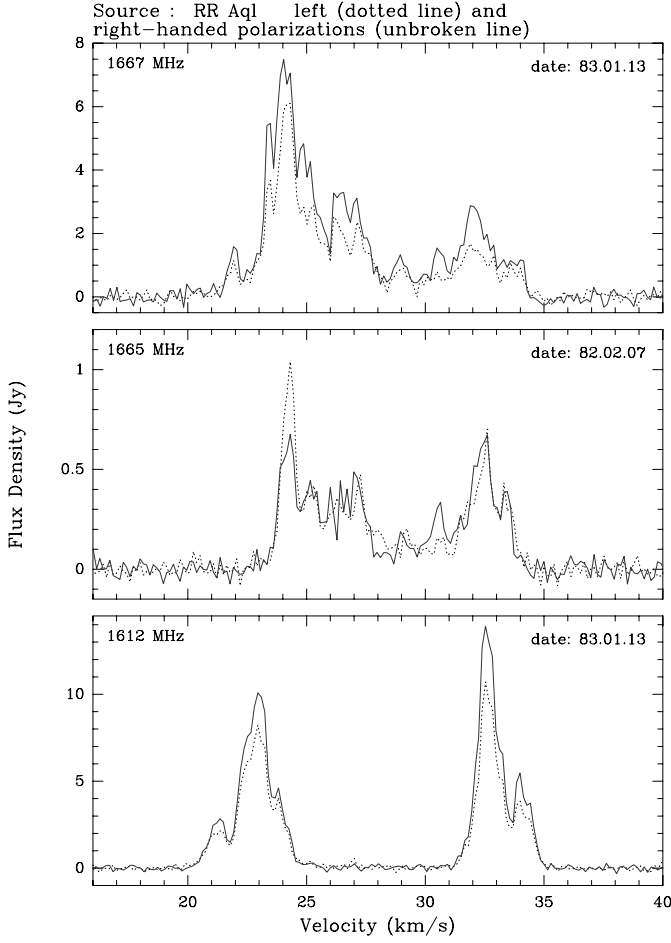
Fig. 6. Spectra of **RR Aql** in the 3 OH maser lines in both circular polarizations

Source : U Her   left (dotted line) and
right-handed polarizations (unbroken line)

Fig. 7. Spectra of **U Her** in both main lines and circular polarizations

Table 4. $\Delta I_{\min-\max}$ for **R Aql**
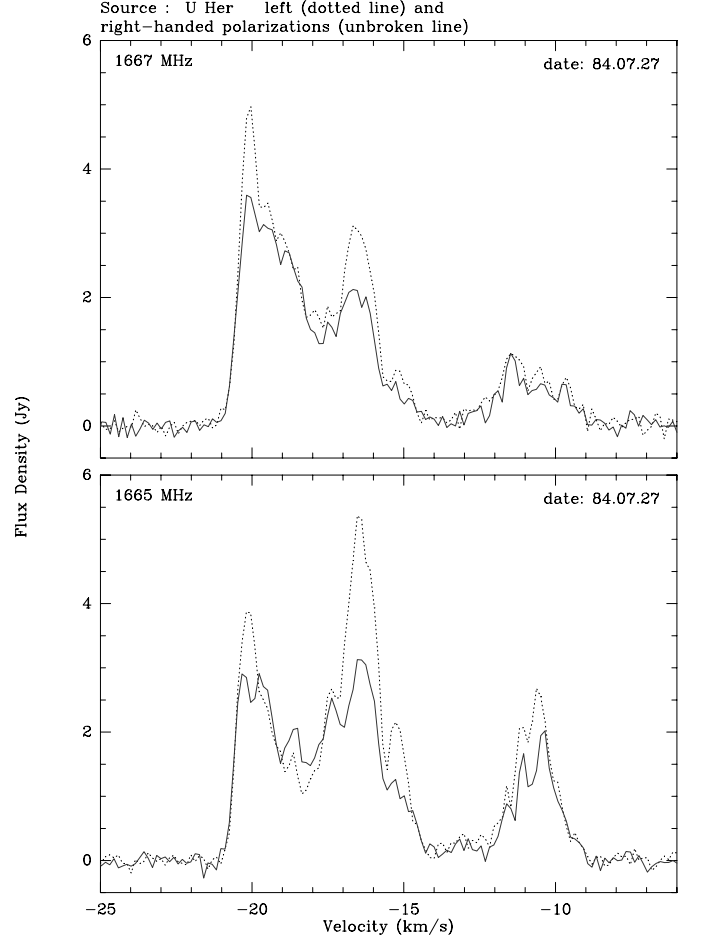
a) $\Delta I_{\min-\max}$ for the integrated flux

Frequency (MHz)	peak	$\Delta I_{\min-\max}$		
		interval 1* polar.		interval 2* polar.
		lin.	cir.	cir.
1612	blue	70%	31%	50%
	red	58%	24%	36%
1667	blue	55, 70%**	71%	48%
	red	60, 82%**	79, 94%**	72%
1665	blue	89, 80%**		
	red	95, 78%**		

b) Range and mean value of $\Delta I_{\min-\max}$ for the components of great longevity

Freq. (MHz)	Peak	$\Delta I_{\min-\max}$			
		Range		Mean Value	
		interval 1*	interval 2*	interval 1	interval 2
1612	blue	10 to 48%	35 to 72%	29%	51%
	red	21 to 31%	25 to 46%	27%	34%
1667	blue	37 to 81%	32 to 58%	62%	43%
	red	45 to 92%	46 to 67%	69%	59%

∗: Same intervals as given Table 3.
∗∗: Respectively for the first and the second cycle observed in this interval of observations.

4.1.3. Spectral components

Figures 10 and 11 display the variations with time of the fitted components at 1612 and 1667 MHz respectively in both circular polarizations for the 2 sets of observations, which correspond in Julian dates to $[45000 - 45400]$ and $[49150 - 49850]$.

The Gaussian fitting of the components brings out the complexity of the blue peak at 1667 as well as at 1612 MHz. One can distinguish 8 and 9 components respectively with a lifetime greater than one stellar period. On the other hand, the red peak shows only 5 and 2 components respectively at 1667 and 1612 MHz (cf. Fig. 2).

Table 4b gives the range and mean value of the $\Delta I_{\min-\max}$ for the intensity of the components exhibiting a longevity greater than one cycle at 1612 and 1667 MHz.

At 1612 MHz the various components are highly stable: they were observed during the whole 15 year span. At this frequency, the blue peak components show a degree of polarization less than 10% except for the one located at $V = +39.55$ km s^{-1} during the second set of observations which shows quite a strong degree of left-handed polarization ([RHC−LHC] $= -0.27$). In contrast
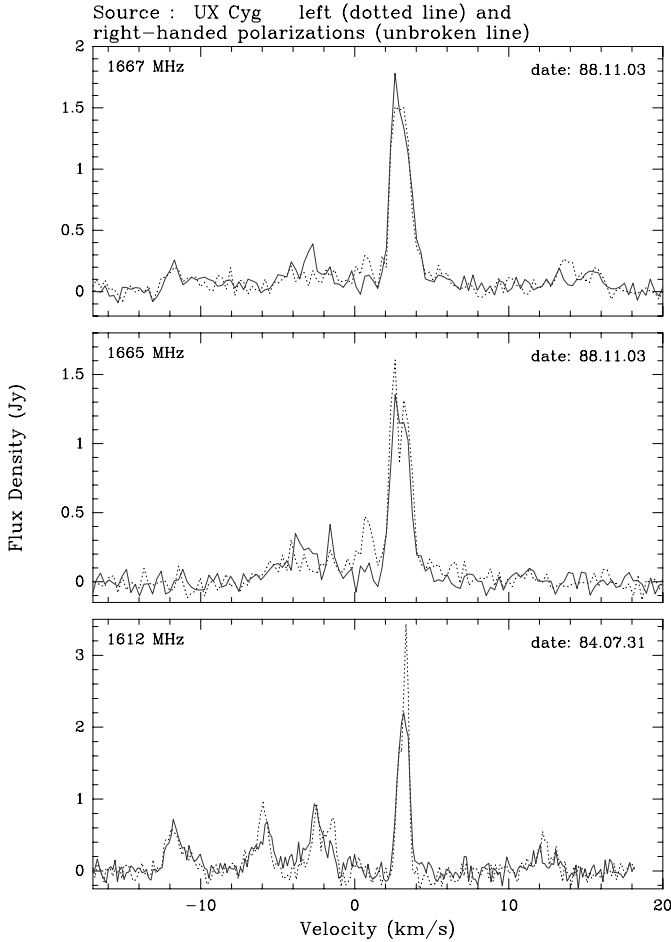
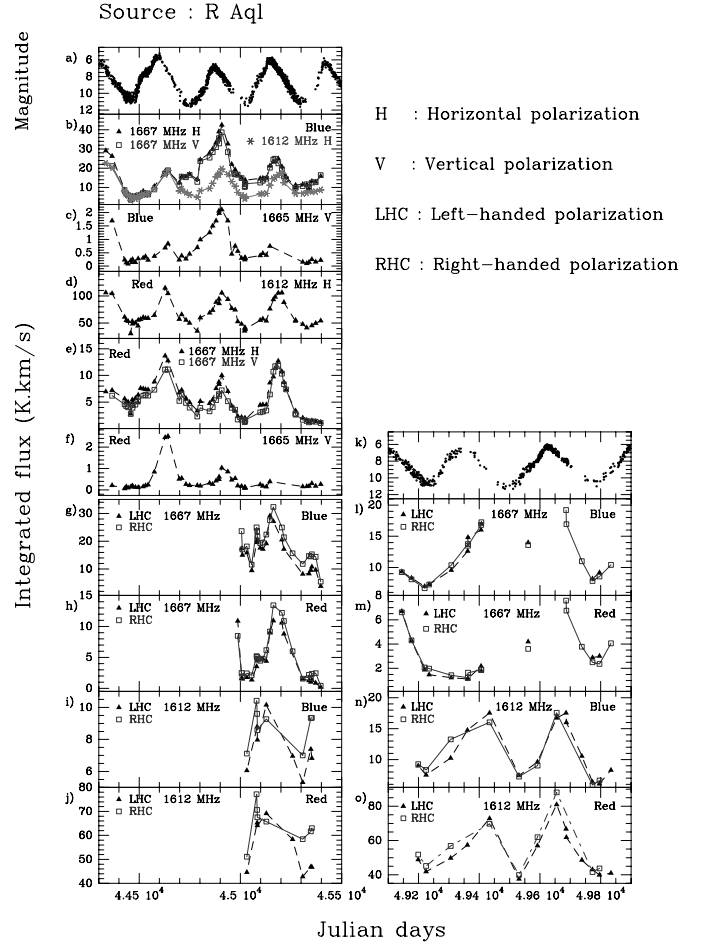**Fig. 8.** Spectra of **UX Cyg** in the 3 OH maser lines and both circular polarizations

Fig. 9. Integrated flux variation curves of **R Aql** in the 3 OH maser lines in linear **b, c, d, e, f** and circular polarization **g, h, i, j** for the first period (i.e., from February 1980 to March 1983) and in circular polarization **l, n, m, o** only for the second period (i.e., from July 1993 to May 1995) for the two standard peaks (labelled Blue and Red in the figure)

both components of the red peak (at $V = +52.91$ km s^{-1} and $V = +54.00$ km s^{-1}) show a degree of right-handed polarization as high as [RHC−LHC] = 0.17 in the first set of observations and less than 10% in the second set.

At 1667 MHz the stability of components is shorter, since some of them disappeared between the first and second set of observations (less than 10 years) while others appeared. At this frequency, the degree of polarization of the whole set of red and blue components is less than 11% for both sets of observations except for the blue component located at $V = +40.78$ km s^{-1} which had a degree of circular polarization as high as [RHC−LHC] = 0.24 during the second set of observations.

One may note that the peak exhibiting the strongest integrated flux (the red peak at 1612 MHz and the blue peak at 1667 MHz) shows a fainter mean value for $\Delta I_{\mathrm{min-max}}$ of the components in comparison with the companion peak for the same line (Table 4).

Thus, there is a correlation between the observed difference in the emission strength between the front and the back part and the degree of saturation in those

regions such that the strongest emission shows the strongest saturation.

4.2. RS Vir

The first set of observations for this star was performed between January 1982 and March 1983 and the second set between May 1993 and June 1994. According to its cyclic periodicity of about 350 days (cf. Table 1), both time spans cover a bit more than a cycle. Unfortunately, the sampling at 1612 MHz for the first set of data is not regular with a gap around the OH minimum. It is regular for the second set, with an observation performed every 1.5 months. The sampling in the main lines for both sets of data is good with, on the average, an observation per month.

Table 5. Central velocity and full width at half-maximum (FWHM) of the fitted components which have shown a longevity greater than 1 stellar period of **RS Vir** at 1612 MHz for the 2 intervals of observations. For comparison are given too in the last column the velocity of the components determined by Herman & Habing (1985, i.e., column labelled H&H)

a) Red peak

	LHC $\mathrm{km\ s^{-1}}$	FWHM $\mathrm{km\ s^{-1}}$	RHC $\mathrm{km\ s^{-1}}$	FWHM $\mathrm{km\ s^{-1}}$	H&H $\mathrm{km\ s^{-1}}$
interval 1[1]	$V_1 = -10.37$	0.859	$V_1 = -10.36$	0.845	-10.25
	$V_2 = -11.31$	0.840	$V_2 = -11.26$	0.771	
interval 2[2]	$V_1 = -10.32$	0.855	$V_1 = -10.31$	0.850	
	$V_2 = -11.25$	0.793	$V_2 = -11.26$	0.735	

b) Blue peak

	LHC $\mathrm{km\ s^{-1}}$	FWHM $\mathrm{km\ s^{-1}}$	RHC $\mathrm{km\ s^{-1}}$	FWHM $\mathrm{km\ s^{-1}}$	H&H $\mathrm{km\ s^{-1}}$
interval 1[1]	$V_1 = -15.41$	0.451	$V_1 = -15.40$	0.453	-15.29
	$V_2 = -16.52$	0.870	$V_2 = -16.52$	0.975	-16.48
	$V_3 = -17.51$	0.527	$V_3 = -17.51$	0.524	-17.53
	$V_4 = -18.27$	0.627	$V_4 = -18.27$	0.606	-18.43[!]
	$V_5 = -18.86$	0.697	$V_5 = -18.82$	0.689	
	$V_6 = -19.75$	0.587	$V_6 = -19.76$	0.525	-19.71
interval 2[2]	$V_1 = -15.37$	0.464	$V_1 = -15.40$	0.467	
	$V_2 = -16.50$	0.900	$V_2 = -16.50$	0.889	
	$V_3 = -17.56$	0.579	$V_3 = -17.54$	0.655	
	$V_4 = -18.25$	0.501	$V_4 = -18.27$	0.505	
	$V_5 = -18.87$	0.750	$V_5 = -18.88$	0.705	
	$V_6 = -19.86$	0.510	$V_6 = -19.85$	0.552	

1: Interval of Julian days $[45000 - 45400]$.
2: Interval of Julian days $[49100 - 49550]$.
!: Corresponding to the mean velocity of components 4 and 5 when there are tightly blended due to lower velocity resolution $(V_4 + V_5)/2 = -18.56 \mathrm{\ km\ s^{-1}}$.

4.2.1. Spectra

Like the previous star, RS Vir is a type II emitter (i.e., strongest at 1612 MHz). Its spectra are displayed in Fig. 3. As can be clearly seen, this star exhibits an intermediate group of components in the main lines which can reach relatively high intensities with respect to the red peak at 1665 MHz.

4.2.2. Integrated flux

In Figs. 12 and 13 are displayed the OH integrated flux variations of the blue, red and intermediate peaks for the 3 maser lines in both circular polarizations.

A general increase of the integrated flux in both main lines is seen, the greatest increase being at 1665 MHz. At 1612 MHz, one can note a rather small increase in the integrated flux of the blue peak and a small decrease for the red peak with approximately the same ratio.

The $\Delta I_{\mathrm{min-max}}$ are the weakest at 1612 MHz, the greatest value being only 46% (i.e., $I_{\mathrm{max}}/I_{\mathrm{min}} \simeq 2.7$). Here again the greatest $\Delta I_{\mathrm{min-max}}$ are observed in the 1665 and 1667 MHz integrated fluxes with respective values of 91% (i.e., $I_{\mathrm{max}}/I_{\mathrm{min}} \simeq 20$) and 89% (i.e., $I_{\mathrm{max}}/I_{\mathrm{min}} \simeq 17$). We can note smaller values of $\Delta I_{\mathrm{min-max}}$ (about $10-15\%$ less) for the second set of observations in comparison with the first set, for the three standard maser line emissions (cf. Table 8).

Two hypotheses can explain this general decrease of $\Delta I_{\mathrm{min-max}}$: (1) a change in the degree of saturation, which in the present case must involve a mechanism affecting the 3 lines simultaneously. The most probable cause is a change in the OH density. (2) A weakening in the radiation of the pumping source shared by the 3 maser lines.

The measurement of the delay between the OH and optical maxima was determined using the second set of data at 1665 MHz. Because of the small amount of data, the optical maximum was measured by the superposition of 2 consecutive cycles for a better definition. The calculated delay is 13 ± 20 days (cf. Table 2). Nevertheless, for first set of data (i.e., Figs. 12d,e,f,h, and i) the delay is about 50–70 days. Thus, the most realistic value for the delay is certainly between the two values, about 30 to 50 days.

The most polarized maser emission is at 1612 MHz (cf. Table 9). The emission at this frequency is right-hand polarized in both data sets. The 1667 MHz maser emission of both standard peaks was also right-hand polarized in the first set, showing a smaller mean value, while the degree of polarization is zero for the whole of second set. The polarization of the standard peaks at 1665 MHz is very weak ($<5\%$) for both data sets.

Table 6. Central velocity and full width at half-maximum (FWHM) of the fitted components which have shown a longevity greater than 1 stellar period of **RS Vir** at 1667 MHz for the 2 intervals of observations

a) Red peak

	LHC km s^{-1}	**FWHM** km s^{-1}	**RHC** km s^{-1}	**FWHM** km s^{-1}
interval 1[1]	$V_1 = -10.18$	1.251	$V_1 = -10.18$	1.265
	$V_2 = -11.38$	1.177	$V_2 = -11.45$	1.111
interval 2[2]	$V_1 = -10.07$	0.944	$V_1 = -10.08$	0.947
	$V_2 = -10.99$	0.847	$V_2 = -10.92$	0.822
	$V_3 = -11.84$	0.896	$V_3 = -11.80$	0.846

b) Intermediate velocity peak

	LHC km s^{-1}	**FWHM** km s^{-1}	**RHC** km s^{-1}	**FWHM** km s^{-1}
interval 1[1]	$V_1 = -13.91$	1.390	$V_1 = -13.91$	1.502
interval 2[2]	$V_1 = -13.47$	1.311	$V_1 = -13.03$	1.022
			$V_2 = -14.14$	1.233

c) Blue peak

	LHC km s^{-1}	**FWHM** km s^{-1}	**RHC** km s^{-1}	**FWHM** km s^{-1}
interval 1[1]	$V_1 = -16.36$	0.899	$V_1 = -16.36$	0.927
	$V_2 = -17.52$	1.016	$V_2 = -17.52$	1.025
			$V_3 = -18.45$	1.021
interval 2[2]	$V_1 = -16.50$	1.061	$V_1 = -16.40$	1.019
	$V_2 = -17.63$	0.928	$V_2 = -17.49$	0.950
	$V_3 = -18.44$	0.876	$V_3 = -18.29$	0.943
	$V_4 = -19.49$	0.967	$V_4 = -19.48$	1.035

1 and 2: Same intervals as given in the previous table.

Table 7. Source: **RS Vir**. The same as for the previous table but for the 1665 MHz

a) Red peak

	LHC km s^{-1}	**FWHM** km s^{-1}	**RHC** km s^{-1}	**FWHM** km s^{-1}
interval 1[1]	$V_1 = -10.25$	0.677	$V_1 = -10.06$	0.677
	$V_2 = -11.11$	0.769	$V_2 = -11.10$	0.956
interval 2[2]	$V_1 = -10.82$	1.111	$V_1 = -10.75$	1.009
	$V_2 = -11.89$	0.933	$V_2 = -11.84$	0.927

b) Intermediate velocity peak

	LHC km s^{-1}	**FWHM** km s^{-1}	**RHC** km s^{-1}	**FWHM** km s^{-1}
interval 1[1]	$V_1 = -13.40$	0.674	$V_1 = -13.23$	0.690
	$V_2 = -14.53$	0.702	$V_2 = -14.64$	0.777
interval 2[2]	$V_1 = -13.26$	0.925	$V_1 = -13.18$	0.854
	$V_2 = -14.51$	0.988	$V_2 = -14.69$	1.186

c) Blue peak

|	**LHC** km s^{-1}	**FWHM** km s^{-1}	**RHC** km s^{-1}	**FWHM** km s^{-1}
interval 1[1]	$V_1 = -16.26$	1.007	$V_1 = -16.34$	0.975
	$V_2 = -17.62$	0.589	$V_2 = -17.65$	0.780
interval 2[2]	$V_1 = -16.41$	1.055	$V_1 = -16.47$	1.037
	$V_2 = -17.69$	0.649	$V_2 = -17.72$	0.679

1 and 2: Same intervals as given in Table 5.
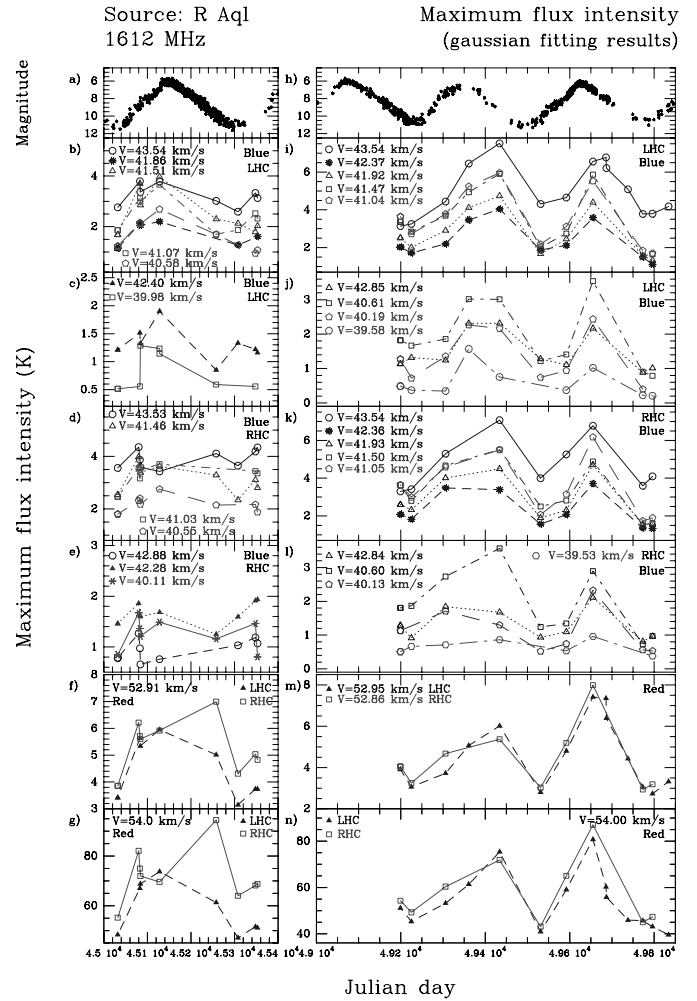
Fig. 10. Intensity variation curves of the Gaussian fitted components of **R Aql** at 1612 MHz in left- (LHC) and right-handed (RHC) polarizations for the red (Red) and blue (Blue) peaks from March 1982 to March 1983 and from July 1993 to May 1995

Table 8. $\Delta I_{\text{min}-\text{max}}$ for the integrated flux of **RS Vir**

Frequency (MHz)	peak	$\Delta I_{\text{min}-\text{max}}$ interval 1*	interval 2*
1612	blue	40%	29%
	red	46%	31%
1667	blue	82%	73%
	red	79%	62%
	intermediate	85%	89%
1665	blue	85%	58%
	red	91%	83%
	intermediate	89%	78%

*: Same intervals as given in Table 5.
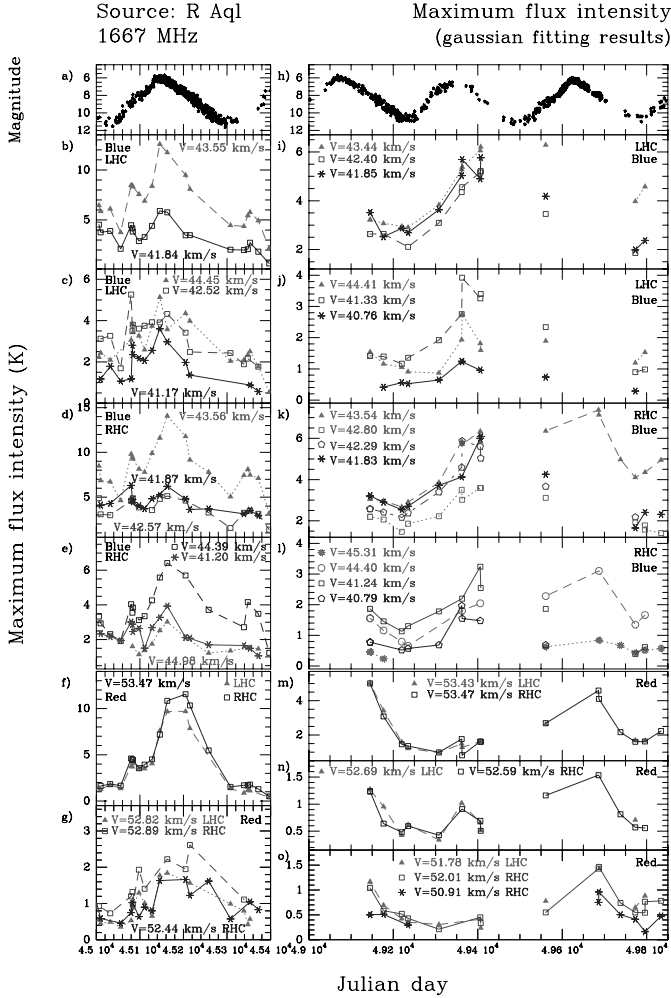
Fig. 11. Intensity variation curves of the Gaussian fitted components of **R Aql** at 1667 MHz in left- (LHC) and right-handed (RHC) polarizations for the red (Red) and blue (Blue) peak from March 1982 to March 1983 and from July 1993 to May 1995

The signal lying between the two standard peaks shows no polarization at all at 1667 MHz for all observations. On the other hand, at 1665 MHz it shows a weak left-handed polarization with a value of $[RHC-LHC]_{1665} = -0.1$ during the OH maximum of the first data set and a very faint right-handed polarization on the second set. This latter behaviour is inverted compared with the standard 1665 MHz emission. Thus, we do not have a correlation between the behaviour of the intermediate and standard peak emission with regard to the polarization, suggesting that the zones concerned with the two emissions possess different characteristics.

4.2.3. Spectral components

Figures 14–17 show the variations during the two epochs of observations of the fitted components respectively at
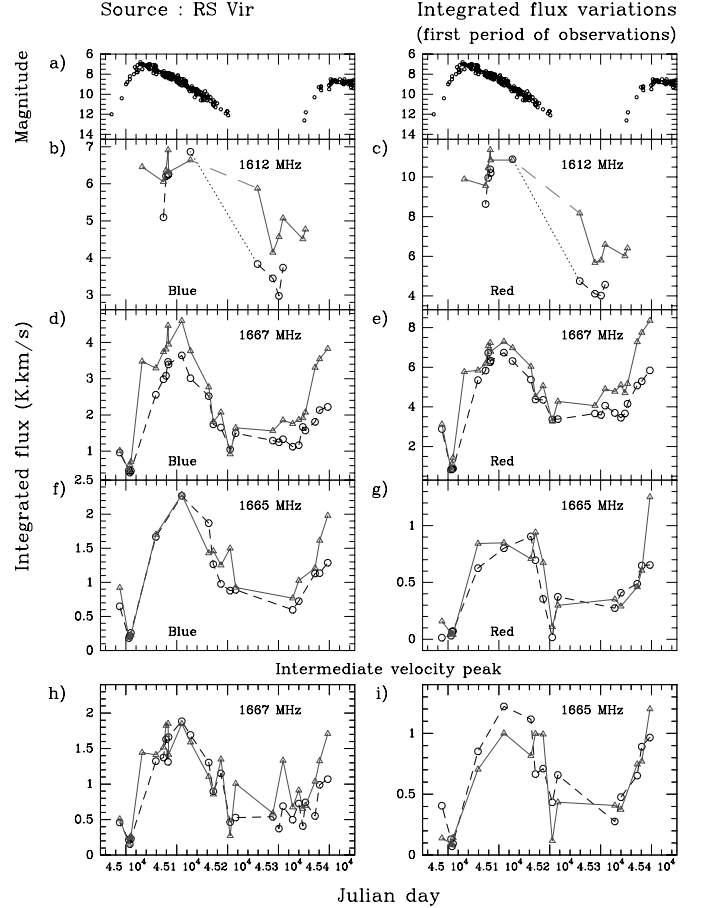
Fig. 12. Integrated flux variation curves of **RS Vir** in the 3 OH maser lines in circular polarization (LHC: circles/RHC: triangles) for the first set of observations (i.e., from January 1982 to March 1983) for the blue (left column i.e., "**b,d,f**" schemes) and red (right column i.e., "**c,e,g**" schemes) standard peaks as well as for the intermediate one ("**h,i**" schemes)

1665, 1667 and 1612 MHz for the 3 peaks (i.e., the blue, the red and the intermediate one) and in both circular polarizations. The complexity of both standard peaks is of the same order in the main lines while a large difference in complexity can be seen between the red and blue peaks at 1612 MHz, the latter exhibiting a great number of components (cf. Fig. 3). Here again component longevity in the main lines is much shorter than in the satellite line. The range and mean value of the $\Delta I_{min-max}$ for the intensity of the components with a longevity greater than one cycle for the three OH maser lines are given Table 10a.

For the main lines, a few components (<4) in both standard peaks show a longevity greater than one cycle. Otherwise, components appear and disappear from one cycle to the next. At 1665 MHz, degrees of polarization exceeding 10% are only observed for 2 components in the first set of observations (cf. Table 10b). At 1667 MHz, none of the components exhibits a degree of polarization greater than 10%. The main line emission of the intermediate peak of this source seems not to have any peculiarity in

Table 9. Mean value of [RHC−LHC] for the standard peak integrated flux of **RS Vir**
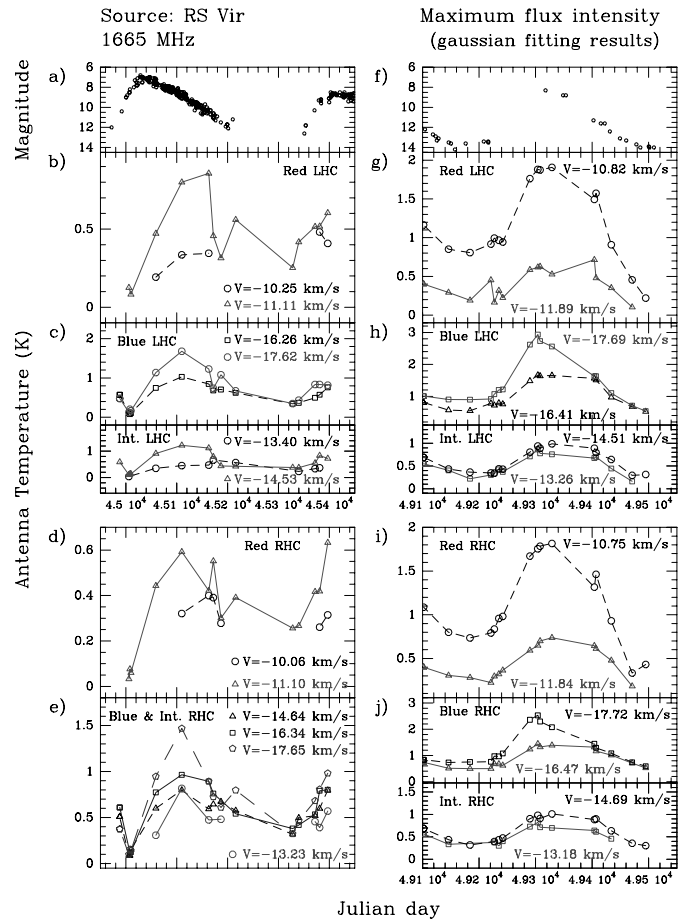
Frequency (MHz)	[RHC−LHC]	
	interval 1*	interval 2*
1612	0.2	0.05
1667	0.1	0
1665	−0.05 < [RHC − LHC] < 0.05	−0.05 < [RHC − LHC] < 0.05

*: Same intervals as given in Table 5.
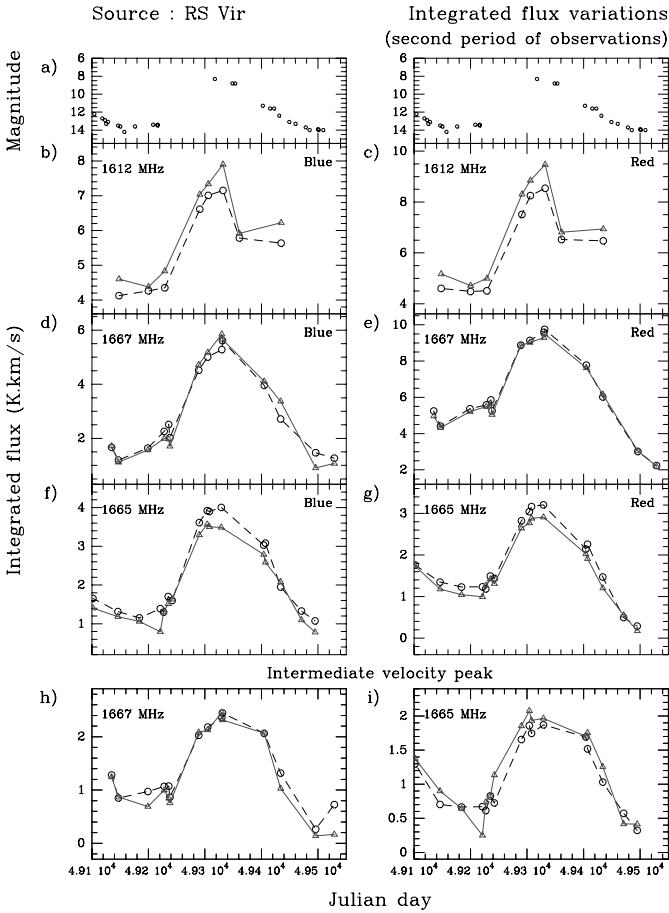
Fig. 13. Source: **RS Vir**. The same as for the previous figure, but for the second set of observations (i.e., from May 1993 to June 1994)

Fig. 14. Intensity variation curves of the Gaussian fitted components of **RS Vir** at 1665 MHz in left- (LHC) and right-handed (RHC) polarizations for the red, blue and intermediade (Int.) peaks from January 1982 to March 1983 and from May 1993 to June 1994

comparison with the blue and red standard peaks. Indeed, its temporal variations are quite similar to both standard peaks and its polarization is about the same.

At 1612 MHz, 6 components in the blue peak and 2 in the red show a long lifetime. At this frequency, the $\Delta I_{\text{min}-\text{max}}$ are quite a bit smaller than in the main lines. Except the component located at $V = -18.84$ km s^{-1} (with [RHC−LHC] = 0.08) all the components with a longevity greater than one stellar cycle contribute to the right-handed polarization observed for the 1612 MHz integrated flux during the first set of observations (cf. Table 10b). During the second set of observations all

components show degrees of polarization smaller than 10% for both peaks.

4.3. S CrB

This source was observed at three different epochs: from January 1982 to March 1983, from January 1986 to July 1987 and from April 1993 to April 1995. During the first interval, the observations in the 1612 MHz satellite line were performed during a stellar period but unfortunately
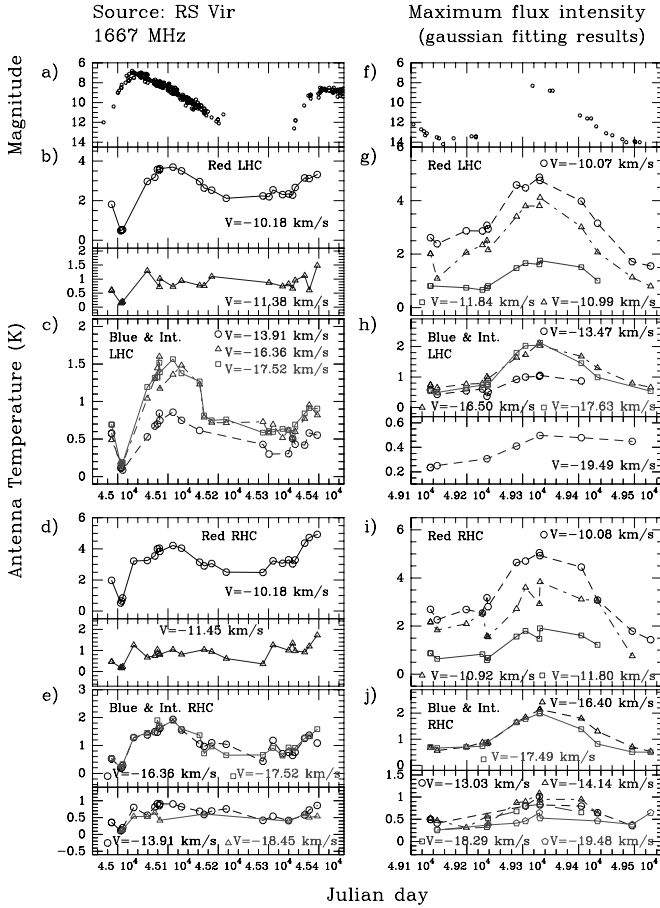
Fig. 15. Source: **RS Vir**. The same as for the previous figure but for the 1667 MHz

centered on an OH minimum; moreover the sampling was not regular. In the main lines, the observations covered almost 1.5 stellar cycles with good sampling: on average an observation every 1.5 month at 1665 MHz and once per month at 1667 MHz. The second epoch covered a bit more than 1.5 cycles. For these data, observations were performed in both circular polarizations only at 1667 MHz while they were performed in the left-handed polarization at 1612 MHz and in the right-handed polarization at 1665 MHz. Finally, during the third epoch the observations cover almost 2 cycles at 1612 MHz and exactly 2 cycles in the main lines. The sampling in the main lines is very good with a separation between two observations less than one month around minima and maxima. In the 1612 MHz satellite line, the sampling is on the average one observation every 1.5 months.

4.3.1. Spectra

Figure 4 shows the spectra of this source in the 3 OH lines and in both circular polarizations. One can see that the most extended spectrum here is at 1667 MHz which extends beyond the 1612 MHz profile by about 2 km s^{-1} for
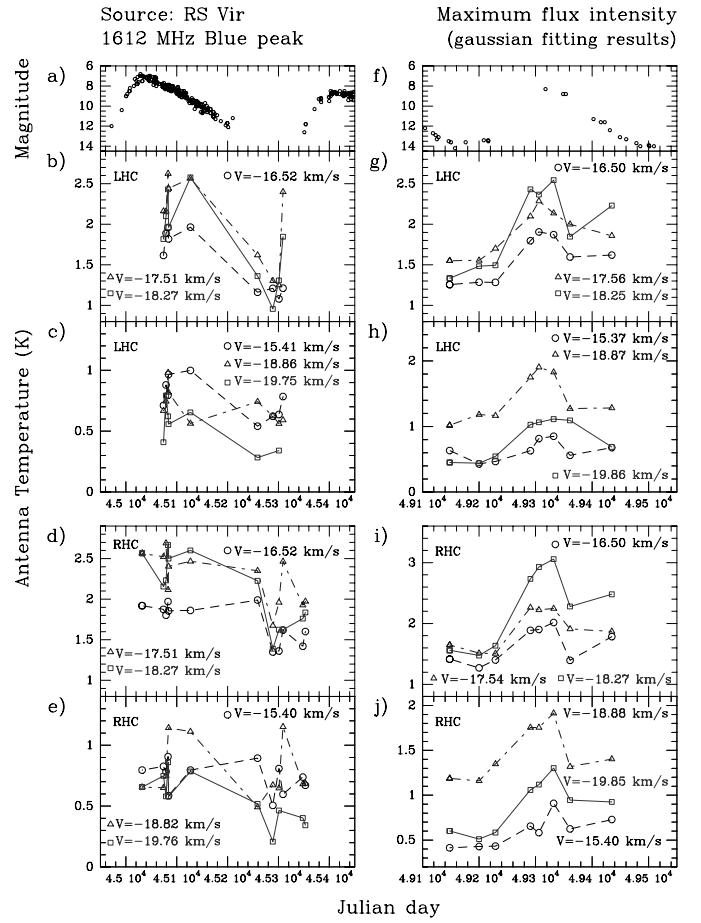
Fig. 16. Intensity variation curves of the Gaussian fitted components of **RS Vir** of the 1612 MHz blue peak in left- (LHC) and right-handed (RHC) polarizations from January 1982 to March 1983 and from May 1993 to June 1994
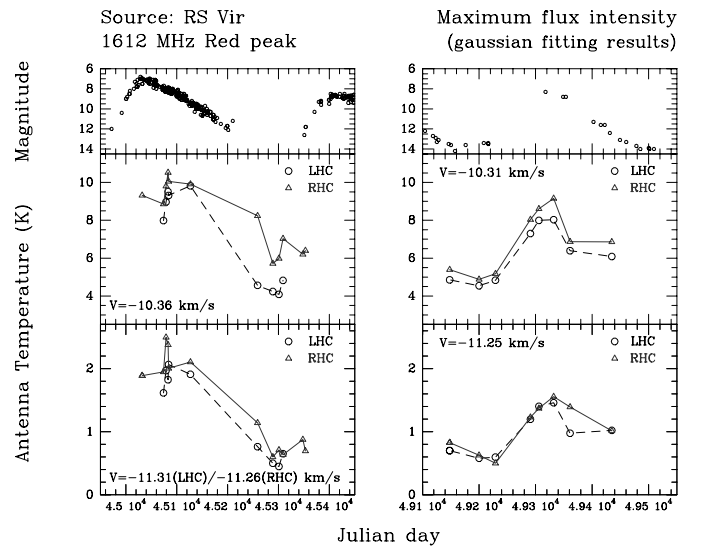
Fig. 17. Source: **RS Vir**. The same as for the previous figure but for the 1612 MHz red peak

Table 10. Results for the components of great longevity of **RS Vir**

a) Range and mean value of $\Delta I_{\min-\max}$

| Freq. (MHz)	Peak	$\Delta I_{\min-\max}$			
		Range		Mean Value	
		interval 1*	interval 2*	interval 1	interval 2
1612	blue	19 to 58%	16 to 43%	34%	29%
	red	30 to 64%	28 to 51%	49%	38%
1667	blue	69 to 86%	36 to 60%	80%	52%
	red	77 to 80%	45 to 67%	78%	57%
	inter.	78 to 81%	42 to 55%	79%	48%
1665	blue	78 to 87%	49 to 69%	84%	58%
	red	21 to 89%	60 to 79%	59%	71%
	inter.	45 to 89%	46 to 68%	74%	55%

*: Same intervals as given in Table 5.

b) $|[RHC-LHC]| \geq 0.10$ for the interval of Julian day $[45000-45400]$

| Freq. (MHz)	peak	$V_{\text{comp.}}$ (km s^{-1})	$[RHC-LHC]$
1612	blue	−15.40	0.25
	blue	−16.52	0.26
	blue	−17.51	0.18
	blue	−18.27	0.24
	blue	−19.75	0.30
	red	−10.36	0.30
	red	−11.26	0.20
1665	red	−11.10	−0.18
	inter.	−14.60	−0.21

the bluest part of the profile and 3 km s^{-1} for the reddest part. Moreover, the shape of the profiles is quite different from one line to another, especially between the main and the satellite lines. Thus, the red peak of the 1667 MHz clearly shows 2 main groups of components, centered respectively at 3.5 and 6.2 km s^{-1}, with a flux ratio of about 2. This ratio is of more than 7 for the 1665 MHz red peak emission. This may be explained by a weaker saturation in the 1665 MHz line than in the 1667 MHz. Moreover, the 1667 MHz blue peak is quite large, with a total spread of about 7 km s^{-1}, showing at least 3 distinct main groups of components of faint intensity. The 1665 MHz blue peak exhibits a flater shape and no predominent groups of components are seen. At 1612 MHz, 3 main groups of components are evident in the blue peak but they are narrower and do not correspond to those at 1667 MHz. This remark is also valid for the 2 main groups of components observed in the 1612 MHz red peak in comparison with the 1667 MHz ones.

4.3.2. Integrated flux

Variations of the integrated flux of the 3 OH maser lines for the 3 epochs of observations are presented Figs. 18 and 19 respectively for the red and the blue peaks.
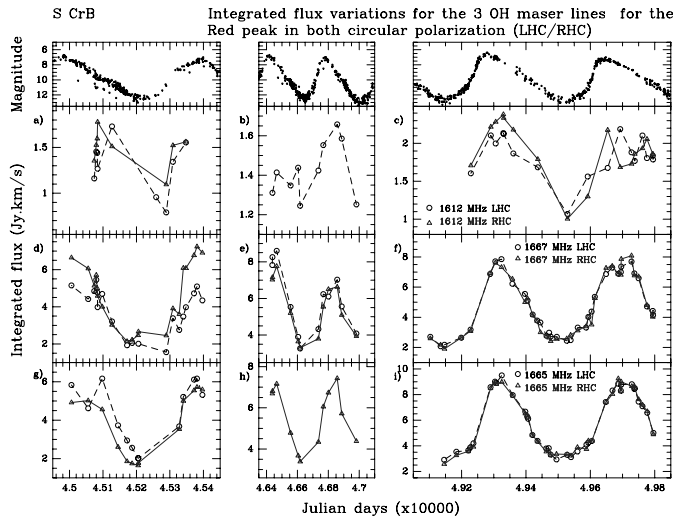
Fig. 18. Integrated flux variation curves of **S CrB** in the 3 OH maser lines in circular polarization from January 1982 to March 1983, from January 1986 to July 1987 and from April 1993 to April 1995 for the red peak. First row (i.e., boxes **a,b,c**): 1612 MHz, second row (i.e., boxes **d,e,f**): 1667 MHz and third row (i.e., boxes **g,h,i**): 1665 MHz
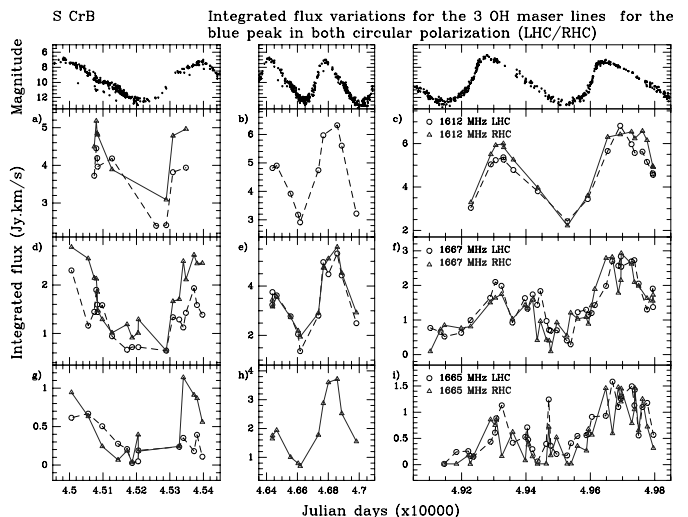
Fig. 19. Source: **S CrB**. The same as for the previous figure, but for blue peak

One can observe the usual phase delay between the OH and optical maxima, calculation gives a value of about 50 ± 10 days (cf. Table 2). Comparing the general shape of the OH and optical curves it is clear that the asymmetry of the OH curves is less than that of the optical curve. This is due to a very small (if any) delay between OH and optical minima in comparison with a distinct delay between the OH and optical maxima. This can be clearly seen Figs. 18f and 18i in comparing with the corresponding part of the optical curve, because of the very good sampling at the OH minima and maxima.

Table 11. Central velocity and full width at half-maximum (FWHM) of the fitted components which have shown a longevity greater than 1 stellar period of **S CrB** at 1612 MHz for each interval of observations

a) Red peak

	LHC km s^{-1}	FWHM km s^{-1}	RHC km s^{-1}	FWHM km s^{-1}
interval 1[1]	$V_1 = 4.31$	0.861	$V_1 = 4.36$	0.777
	$V_2 = 3.21$	0.734	$V_2 = 3.20$	0.757
interval 2[2]	$V_1 = 4.29$	0.830	(*)	
	$V_2 = 3.20$	0.897		
interval 3[3]	$V_1 = 4.24$	0.879	$V_1 = 4.23$	0.814
	$V_2 = 3.04$	0.653	$V_2 = 3.05$	0.723

b) Blue peak

	LHC km s^{-1}	FWHM km s^{-1}	RHC km s^{-1}	FWHM km s^{-1}
interval 1[1]	$V_1 = -2.21$	0.638	$V_1 = -2.24$	0.674
	$V_2 = -2.94$	0.761	$V_2 = -3.02$	0.709
	$V_3 = -3.89$	0.956	$V_3 = -3.92$	0.966
interval 2[2]	$V_1 = -2.15$	0.647		
	$V_2 = -2.94$	0.890	(*)	
	$V_3 = -4.13$	0.765		
interval 3[3]	$V_1 = -2.26$	0.587	$V_1 = -2.29$	0.658
	$V_2 = -3.02$	0.738	$V_2 = -3.10$	0.669
	$V_3 = -4.14$	0.658	$V_3 = -4.15$	0.623

1: Interval of Julian days [45000 − 45400].
2: Interval of Julian days [46400 − 47000].
3: Interval of Julian days [49100 − 49800].
(*): No observations at this polarization for this period.

The variations of integrated flux amplitude from one cycle to another are here again quite similar for both main lines. Large variations in the values of the integrated flux maxima in the blue peak at 1665 as well as at 1667 MHz across all 3 epochs of observations are seen. The ratio of greatest value reached by the OH maximum to the smallest in the blue peak is 4 and 2-3 respectively at 1665 and 1667 MHz while a weaker ratio was measured in the red peak, less than 1.6 and 1.2 respectively at 1665 and 1667 MHz. On the other hand, the value of the integrated flux maxima at 1612 MHz did not change by more than a factor of 1.3 for both standard peaks.

The values of $\Delta I_{\mathrm{min-max}}$ are given Table 14. Notice that the $\Delta I_{\mathrm{min-max}}$ of the integrated flux in both main lines were about the same and systematically greater than in the 1612 MHz satellite line. Further more, the greatest values of $\Delta I_{\mathrm{min-max}}$ in each line were all observed for the blue peak integrated flux while the faintest, observed in the second set of observations (i.e., interval of Julian days [46400 − 47000]), were all obtained for the red peak.

From the first and third interval of observations, for which both circular polarizations are available, the 1612 MHz emission was mainly weakly right-hand polarized. The 1667 MHz emission has shown a change in its behaviour, since it was first right-hand polarized with a degree of circular polarization reaching a value

Table 12. Source: **S CrB**. The same as for the previous table but for the 1667 MHz

a) Red peak

	LHC km s^{-1}	FWHM km s^{-1}	RHC km s^{-1}	FWHM km s^{-1}
interval 1[1]	$V_1 = 7.23$	0.629	$V_1 = 7.12$	0.711
	$V_2 = 5.93$	0.830	$V_2 = 5.88$	0.831
	$V_3 = 5.02$	0.660	$V_3 = 5.16$	0.554
			$V_4 = 4.67$	0.803
	$V_5 = 4.22$	0.802	$V_5 = 4.09$	0.763
	$V_6 = 3.35$	0.956	$V_6 = 3.34$	0.928
interval 2[2]	$V_1 = 5.82$	0.817	$V_1 = 5.82$	0.879
	$V_2 = 4.50$	1.003	$V_2 = 4.48$	1.015
	$V_3 = 3.39$	0.927	$V_3 = 3.36$	0.938
interval 3[3]	$V_1 = 6.34$	0.419	$V_1 = 6.27$	0.345
	$V_2 = 5.76$	0.603	$V_2 = 5.78$	0.537
	$V_3 = 5.30$	0.430	$V_3 = 5.23$	0.451
	$V_4 = 4.68$	0.619	$V_4 = 4.67$	0.551
	$V_5 = 3.74$	0.956	$V_5 = 3.89$	0.843
	$V_6 = 2.92$	0.782	$V_6 = 3.04$	0.826

b) Blue peak

	LHC km s^{-1}	FWHM km s^{-1}	RHC km s^{-1}	FWHM km s^{-1}
interval 1[1]	$V_1 = -0.86$	1.071	$V_1 = -0.80$	1.197
	$V_2 = -2.44$	1.333	$V_2 = -2.42$	1.435
interval 2[2]	$V_1 = -0.71$	1.215	$V_1 = -0.59$	1.204
	$V_2 = -2.41$	1.590	$V_2 = -2.39$	1.512
	$V_3 = -4.35$	1.242	$V_3 = -4.08$	1.280
	$V_4 = -6.03$	1.299	$V_4 = -6.01$	1.314
interval 3[3]	(*)		(*)	

1,2 and 3: Same intervals as given in the previous table.
(*): No fitting for this period due to the faintness of the signal.

Table 13. Source: **S CrB**. The same as for the previous table but for the 1665 MHz

a) Red peak

	LHC km s^{-1}	FWHM km s^{-1}	RHC km s^{-1}	FWHM km s^{-1}
interval 1[1]	$V_1 = 4.41$	0.480		
	$V_2 = 3.90$	0.412	$V_2 = 4.04$	0.696
	$V_3 = 3.31$	0.788	$V_3 = 3.21$	0.812
interval 2[2]	(*)		$V_1 = 4.85$	0.552
			$V_2 = 4.05$	0.754
			$V_3 = 3.14$	0.938
interval 3[3]	$V_1 = 5.29$	0.542	$V_1 = 5.30$	0.454
	$V_2 = 4.61$	0.484	$V_2 = 4.72$	0.507
	$V_3 = 3.75$	0.741	$V_3 = 3.93$	0.782
	$V_4 = 2.94$	0.844	$V_4 = 3.03$	0.917

1, 2 and 3: Same intervals as given in the Table 11.
(*): No observations at this polarization for this period.
b) Blue peak.

No fitting were made for the third period for this peak due to the faintness of the signal.

Table 14. $\Delta I_{\min-\max}$ for the integrated flux of **S CrB**

Frequency (MHz)	peak	$\Delta I_{\min-\max}$ interval 1*	interval 2*	interval 3*
1612	blue	30%	37%	50%
	red	37%	14%	41%
1667	blue	60%	59%	81%
	red	54%	45%	58%
1665	blue	73%	69%	79%
	red	55%	37%	54%

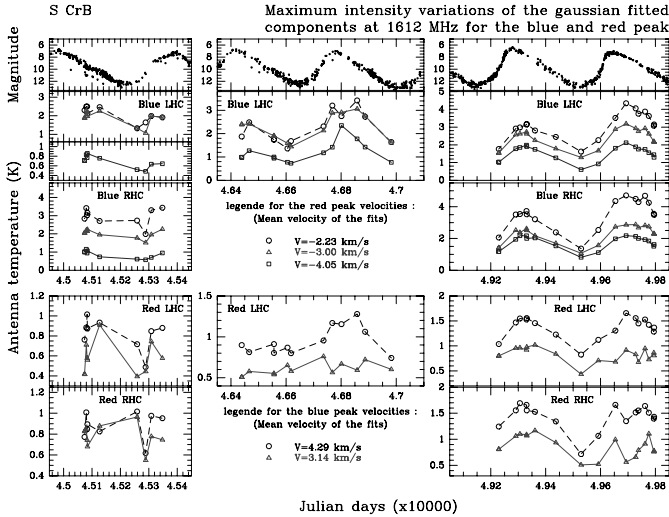∗: Same intervals as given in the Table 11.

Fig. 20. Intensity variation curves of the Gaussian fitted components of **S CrB** at 1612 MHz in left- (LHC) and right-handed (RHC) polarizations for the two standard peaks for the 3 sets of observations (i.e., from January 1982 to March 1983, from January 1986 to July 1987 and from April 1993 to April 1995)

of $[\text{RHC}-\text{LHC}]_{1667} = 0.2$ in the first data set while it shows no degree of polarization for the second and third sets of data for both standard peaks. As for the 1667 MHz, the 1665 MHz line shows polarized emission for the first data set and no degree of polarization for third. But, contrarily to the 1667 MHz, the behaviour at 1665 MHz is different for the red and blue peaks. Indeed, while the red 1665 MHz peak emission shows a faint left-handed polarization (with the strongest value of about $[\text{RHC}-\text{LHC}]_{1665} = -0.15$) in the first set of observations, the blue 1665 MHz peak emission shows a right-handed polarization with a maximum value $[\text{RHC}-\text{LHC}]_{1665} = 0.33$ during the second maximum around the Julian day 45340.

4.3.3. Spectral components

Figures 20–23 display the temporal variations of the various fitted spectral components in the 3 OH maser lines, for the 3 epochs. At 1612 MHz, all the components detected in the first data set could be observed in the next two
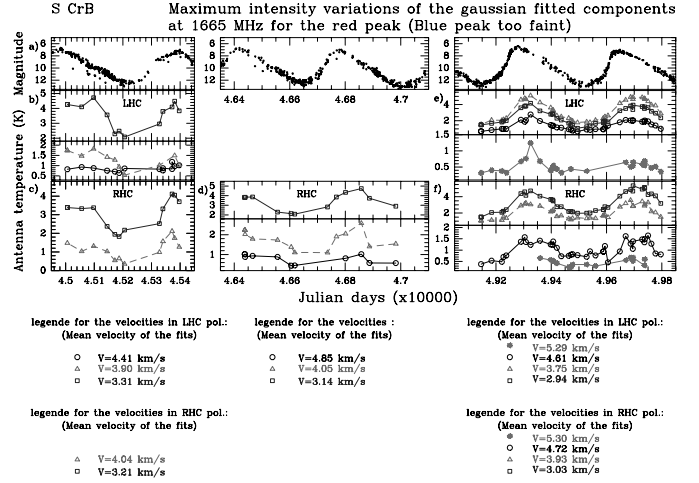

Fig. 21. Source: **S CrB**. The same as for the previous figure but for the 1665 MHz red peak. The blue peak was too faint for a reasonably good fitting
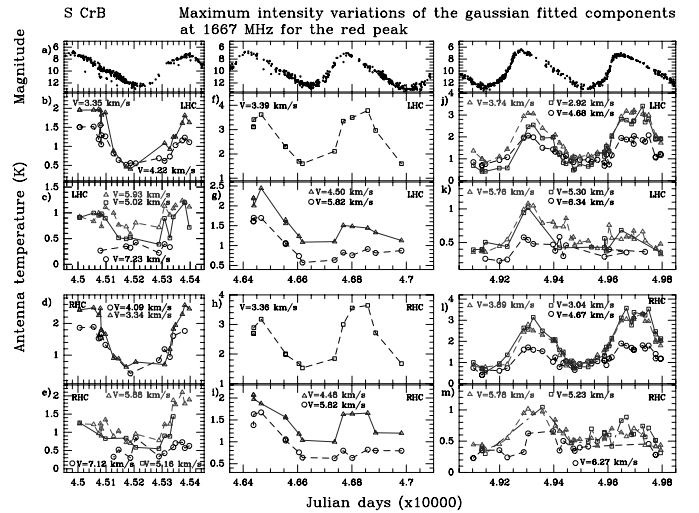

Fig. 22. Intensity variation curves of the Gaussian fitted components of **S CrB** at 1667 MHz in left- (LHC) and right-handed (RHC) polarizations for the red peak for the 3 set of observations (i.e., from January 1982 to March 1983, from January 1986 to July 1987 and from April 1993 to April 1995)

epochs. Thus for this line, (i.e., Fig. 20) and for simplicity, only the mean value of the velocity of each component is given because of their great stability.

The range and mean value of the intensity $\Delta I_{\min-\max}$ for those components exhibiting a longevity greater than one cycle for the three OH maser lines are given Table 15a. At 1612 MHz, the ranges of amplitudes of variations are systematically greater for the blue peak components than for those of the red peak. This can be interpreted as a greater degree of saturation for the 1612 MHz emission coming from the back part of the shell than from the front. This behaviour clearly demonstrates the inhomogeneity between the front and the back parts of the shell.
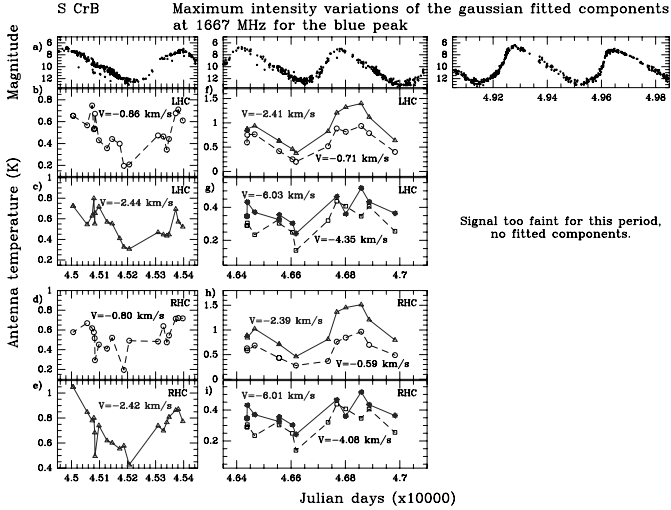
Fig. 23. Source: **S CrB**. The same as for the previous figure but for the blue peak
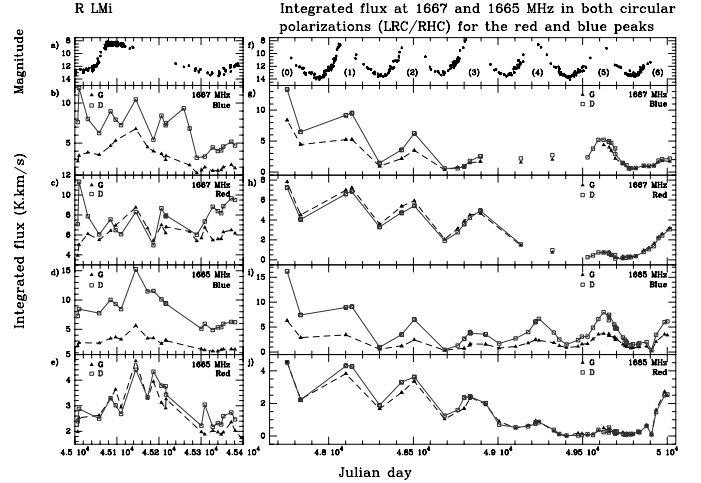

Fig. 24. Integrated flux variation curves of **R LMi** in both main lines and circular polarizations from January 1982 to March 1983 and from August 1989 to November 1995

The ||[RHC−LHC]| ≥ 0.10 for the components of great longevity are given in Table 15b. We note that the behaviour of the components with regard to the polarization is quite different from one line to another, and surprisingly between both main lines. Even though the integrated flux at 1667 MHz for both standard peaks exhibits a degree of circular polarization greater than 10% in the first interval of observations, none of the components with a great longevity in the blue peak shows ||[RHC−LHC]| > 0.10. On the contrary, while the red peak integrated flux at 1665 MHz shows [RHC−LHC] = 0 in the third interval of observations, three spectral components with a great longevity appear to be strongly polarized (Table 15b).

4.4. R LMi

R LMi was observed during one stellar period between January 1982 and March 1983 and during almost 6 consecutive cycles from August 1989 to November 1995. This star is a type I emitter and, up to June 1994, no significant 1612 MHz emission could be detected. The eruptive 1612 MHz emission was studied by Etoka & Le Squeren (1997); thus, only the maser emission of the main lines is presented here.

4.4.1. Spectra

The spectra in both main lines and circular polarizations are displayed Fig. 5. It is clear that at the date of the displayed observations a rather strong right-handed polarization, for the blue peak, was observed. Also the spectral profile, the range of emission as well as the maximum detected intensity are roughly similar for both main lines. In particular, each of the two peaks shows two well defined main groups of components centered about the same velocity.

4.4.2. Integrated flux

The integrated flux variations for the two epochs of observations and for both main lines are displayed Fig. 24. The consecutive cycles of the second interval of observations are labelled from (0) to (6). The phase delay between the OH and the optical curve is 52 ± 15 days (cf. Table 2). From the 6 consecutive cycles, one can see a slow decline of the mean integrated flux value followed by a slow increase for the maser emission of the two peaks at 1665, as well as at 1667 MHz. Clearly, the variation of the mean value of the integrated flux from one cycle to another is not a random process but undergoes a slow variation over several cycles. Moreover, the 1665 MHz emission indicates that this long-term variation is roughly the same for the front and back part of the shell. Nevertheless, the minimum of the red peak long-term variation was delayed of 2 cycles compared to the blue peak one. Unfortunately, due to undersampling at 1667 MHz at the end of the OH cycle (3) and during the OH cycle (4), we can not certify that this trend was exactly the same in this line, even though the behaviour from cycles (0) to (3) and from cycles (5) and (6) are identical for a specific peak in both main lines.

The values of $\Delta I_{\min-\max}$ are given in Table 18. For the second set of observations, which covers 6 consecutive cycles, $\Delta I_{\min-\max}$ ranged from 36% to 93% with a mean value of 66% for the 1667 MHz line. They were slightly greater at 1665 MHz, ranging from 39% to 95% with a mean value of 72.5%. Moreover, there is an increase in the amplitude of variation while the mean integrated flux value decreases (i.e., from cycle (1) to (2) in the case of the blue peak and from cycle (1) to (4) for the red peak).

Table 15. Results for the components of great longevity of **S CrB**

a) Range and mean value of $\Delta I_{\min-\max}$

Freq. (MHz)	Peak	$\Delta I_{\min-\max}$					
		Range			Mean Value		
		interval 1*	interval 2*	interval 3*	interval 1	interval 2	interval 3
1612	blue	19 to 36%	36 to 53%	33 to 55%	27%	44%	45%
	red	24 to 40%	20 to 27%	33 to 40%	31%	23%	37%
1667	blue	42 to 58%	36 to 58%		50%	49%	
	red	31 to 66%	14 to 50%	43 to 75%	49%	33%	53%
1665	blue						
	red	30 to 71%	39 to 40%	46 to 61%	47%	39%	53%

b) |[RHC−LHC]| ≥0.10

| freq. MHz	peak	V_{comp} (km s^{-1})	interval *	[RHC−LHC]
1612	blue	−2.23	1	$\simeq 0.15$
	blue	−4.05	1	$\simeq 0.15$
	red	+3.14	1!	0.42
	red	+4.29	1!	0.17
1667	red	all comp.	1	> 0.10
	red	+5.90	1	0.26
	red	+7.20	1	0.26
1665	red	+3.00	3	0.06, 0.15**
	red	+3.80	3	< −0.24, −0.15**
	red	+4.65	3	< −0.24, −0.15**

∗: Same intervals as given in the Table 11.

!: Around the Julian day 45260 framing an OH minimum.

∗∗: Respectively for the first and second cycle of the third interval.

From Fig. 24, we note that the behaviour concerning the polarization is similar for the two main lines. Thus, while an almost zero polarization can be observed in both main lines for the red peak, a rather strong right-handed polarization is observed for the blue peak in both main lines. The degree of polarization for the blue peak reaches values higher than 0.45 in both lines in the very first set of data (cf. Table 19).

4.4.3. Spectral components

Figures 25 and 26 display the variations in intensity of the fitted red and blue peak components with the longest lifetime at 1665 and 1667 MHz respectively. From a comparison between the variability curves of the first (i.e., for the Julian days [45000 − 45400]) and the second (i.e., for the Julian days [47700 − 50050]) data sets it appears that the mean lifetime of the components can be greater than 5 cycles but less than 10 years. On average, in each peak, only 2 components have a longevity greater than 10 years at 1665 and at 1667 MHz. On the other hand, components with short lifetime can be rather numerous, more than 5 for a given peak can be observed during the very first cycle lying in the interval of Julian days [45000 − 45400].
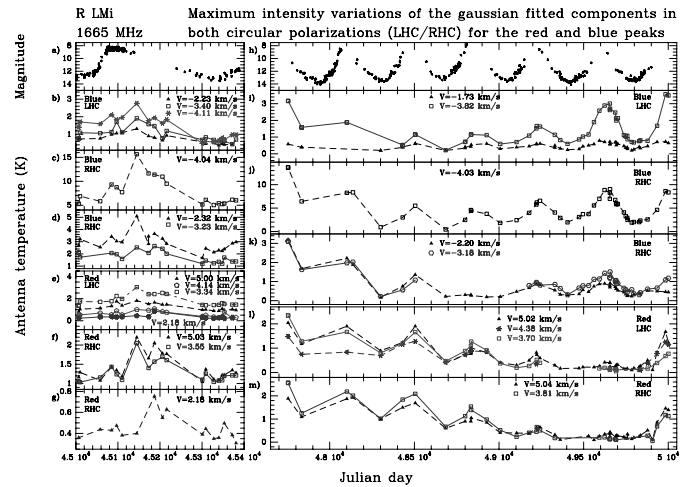
Fig. 25. Intensity variation curves of the Gaussian fitted components of **R LMi** at 1665 MHz in left- (LHC) and right-handed (RHC) polarizations for the red and blue peaks for the two epochs of observations (i.e., from January 1982 to March 1983 and from August 1989 to November 1995)

Moreover, Figs. 25i and 26g,h and j clearly show that for this star, the degree of saturation differs from one component to another. Indeed, some of them exhibit large flux variations from one cycle to another while others undergo variations of the same order of magnitude.

Table 16. Central velocity and full width at half-maximum (FWHM) of the fitted components which have shown a longevity greater than 1 stellar period of **R LMi** at 1667 MHz for each interval of observations

a) Red peak

	LHC $\mathrm{km\ s^{-1}}$	FWHM $\mathrm{km\ s^{-1}}$	RHC $\mathrm{km\ s^{-1}}$	FWHM $\mathrm{km\ s^{-1}}$
interval 1[1]	$V_1 = 6.01$	0.527	$V_1 = 5.95$	0.568
	$V_2 = 4.93$	0.723	$V_2 = 4.98$	0.754
	$V_3 = 4.15$	0.721	$V_3 = 4.07$	0.629
	$V_4 = 3.39$	0.687	$V_4 = 3.41$	0.641
	$V_5 = 2.59$	0.705	$V_5 = 2.59$	0.625
interval 2[2]	$V_1 = 5.79$	0.529	$V_1 = 5.87$	0.496
	$V_2 = 4.95$	0.729	$V_2 = 5.03$	0.731
	$V_3 = 4.36$	0.541		
	$V_4 = 3.80$	0.713	$V_4 = 3.99$	0.698
	$V_5 = 2.90$	0.647	$V_5 = 3.01$	0.720

b) Blue peak

	LHC $\mathrm{km\ s^{-1}}$	FWHM $\mathrm{km\ s^{-1}}$	RHC $\mathrm{km\ s^{-1}}$	FWHM $\mathrm{km\ s^{-1}}$
interval 1[1]	$V_1 = -2.37$	0.833	$V_1 = -2.45$	0.726
	$V_2 = -3.33$	0.633	$V_2 = -3.21$	0.568
	$V_3 = -4.13$	0.825	$V_3 = -4.06$	0.651
	$V_4 = -4.96$	0.521	$V_4 = -4.86$	0.685
interval 2[2]	$V_1 = -1.83$	0.737	$V_1 = -1.82$	0.871
	$V_2 = -2.65$	0.775	$V_2 = -2.48$	0.609
	$V_3 = -3.17$	0.653	$V_3 = -3.13$	0.714
	$V_4 = -3.96$	0.807	$V_4 = -3.97$	0.746

1: Interval of Julian days $[45000 - 45400]$.
2: Interval of Julian days $[47700 - 50050]$.

Table 17. Source: **R LMi**. The same as for the previous table but for the 1665 MHz

a) Red peak

	LHC $\mathrm{km\ s^{-1}}$	FWHM $\mathrm{km\ s^{-1}}$	RHC $\mathrm{km\ s^{-1}}$	FWHM $\mathrm{km\ s^{-1}}$
Interval 1[1]	$V_1 = 5.00$	0.714	$V_1 = 5.03$	0.812
	$V_2 = 4.14$	0.567	$V_2 = 4.23$	0.561
	$V_3 = 3.34$	0.628	$V_3 = 3.55$	0.934
	$V_4 = 2.18$	0.608	$V_4 = 2.18$	0.681
Interval 2[2]	$V_1 = 5.02$	0.657	$V_1 = 5.04$	0.682
	$V_2 = 4.38$	0.525		
	$V_3 = 3.70$	0.659	$V_3 = 3.81$	0.683
	$V_4 = 3.01$	0.696	$V_4 = 2.94$	0.691
	$V_5 = 2.30$	0.824	$V_5 = 2.38$	0.589

b) Blue peak

	LHC $\mathrm{km\ s^{-1}}$	FWHM $\mathrm{km\ s^{-1}}$	RHC $\mathrm{km\ s^{-1}}$	FWHM $\mathrm{km\ s^{-1}}$
Interval 1[1]	$V_1 = -2.23$	0.770	$V_1 = -2.32$	0.715
	$V_2 = -3.40$	0.731	$V_2 = -3.23$	0.575
	$V_3 = -4.11$	0.708	$V_3 = -4.04$	0.517
Interval 2[2]	$V_1 = -1.73$	1.031	$V_1 = -2.20$	0.752
			$V_2 = -3.18$	0.590
	$V_3 = -3.82$	0.813	$V_3 = -4.03$	0.583

1 and 2: Same intervals as given in the previous table.

Table 18. $\Delta I_{\mathrm{min-max}}$ for the integrated flux of **R LMi**

Freq. (MHz)	peak	$\Delta I_{\mathrm{min-max}}$						
		interval 1[a]	interval 2[b]					
			(1)	(2)	(3)	(4)	(5)	(6)
1667	blue	65%	74%	83%	>63%		80%	>59%
	red	38%	36%	48%	52%		73%	>93%
1665	blue	57%	81%	87%	80%	63%	71%	>63%
	red	41%	39%	49%	64%	93%	86%	>95%

a: Interval of Julian days $[45000 - 45400]$.
b: Interval of Julian days $[47700 - 50050]$ covering 6 consecutive cycles labelled from (0) to (6) in Fig. 24.
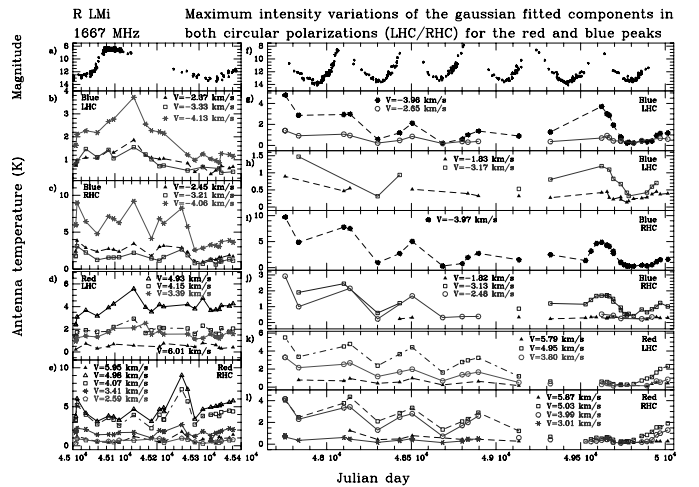
Table 19. [RHC−LHC] for the blue peak integrated flux of **R LMi** in both main lines
a) Interval of Julian days $[45000 - 45400]$

Frequency (MHz)	[RHC−LHC]
1667	$+0.20 \leq$ [RHC−LHC] $\leq +0.46$
1665	$+0.50 \leq$ [RHC−LHC] $\leq +0.60$

b) Interval of Julian days $[47700 - 50050]$ covering 6 consecutive cycles labelled from (0) to (6) in Fig. 24

Frequency (MHz)	[RHC−LHC]					
	(0)	(1)	(2)	(3)	(4)	(5)
1667	+0.23	+0.29	+0.28			+0.10
1665	+0.44	+0.45	+0.45	+0.42	+0.45	+0.37

Fig. 26. Source: **R LMi**. The same as for the previous figure but at 1667 MHz

Table 20 gives the range and mean values of $\Delta I_{\mathrm{min-max}}$ of the components of the blue and red peaks for both main lines observed over at least one cycle in the first set of observations. Table 21 gives the trend of $\Delta I_{\mathrm{min-max}}$ for those components with the greatest longevity over the 5 concecutive cycles of the second set of observations labelled from (1) to (5) in Fig. 24 for both the 1665 and 1667 MHz. Finally, in Table 22 are listed the components for which $|[\mathrm{RHC-LHC}]| \geq 0.10$.

Table 20. Range and mean value of the $\Delta I_{\mathrm{min-max}}$ for the components of great longevity of **R LMi** for the first set of observations (i.e., interval of Julian days [45000 − 45400])

Freq. (MHz)	peak	$\Delta I_{\mathrm{min-max}}$	
		range	mean value
1667	blue	56 to 66%	59%
	red	37 to 69%	52%
1665	blue	38 to 70%	55%
	red	33 to 65%	45%

Table 21. Range and mean value of the $\Delta I_{\mathrm{min-max}}$ for the components of great longevity of **R LMi** for the five cycles labelled from (1) to (5) of the second set of observations (i.e., interval of Julian days [47700 − 50050])

Freq. (MHz)	peak	$V_{\mathrm{comp.}}$ (km s^{-1})	$\Delta I_{\mathrm{min-max}}$ cycle				
			(1)	(2)	(3)	(4)	(5)
1667	blue	all comp.[1]	71%	78%	77%		56%
	red	all comp.[2]	43%	49%	48%		54%
1665	blue	$-2.20, -3.20, -4.05$	80%	↘		55%	65%
	blue	$-1.75, -3.80$	<60%	↘		45%	65%
	red	$+3.75$	35%	↗	73%	↘	<44%
	red	$+5.00$	33%	56%	50%	68%	58%

1: The real values are within a range of $\pm$ 10% from the given mean values for cycles (1) and (2) while within a range of $\pm$ 32% for cycle (3) and (5).
2: The real values are within a range of $\pm$ 15% from the given mean values.

4.5. RR Aql

This star was observed during two different epochs. The first set of observations was performed between January 1982 and March 1983. With its period of 394 days (cf. Tables 1 and 2), this interval covers one cycle. The second set of data was performed from July 1993 to April 1995 and covers a bit less than 2 cycles.

4.5.1. Spectra

For this star as for RS Vir, maser emission occurs between the red and blue peaks (cf. Fig. 6). According to the shape of the main line spectra, with rather blended components, only the small group centered at $V = +29.00$ km s^{-1} has been considered as an intermediate peak. In comparison with the 1612 MHz profile, the two adjacent groups of components in both main line profiles (i.e., at [+26.0; +28.0] km s^{-1} and [+29.7; +31.0] km s^{-1}) could be considered as belonging to the intermediate peak, but as they are usually blended with the blue and red peaks respectively, they have been treated as part of them.

4.5.2. Integrated flux

Figure 27 shows the integrated flux variations in the 3 OH maser lines in both circular polarizations for the
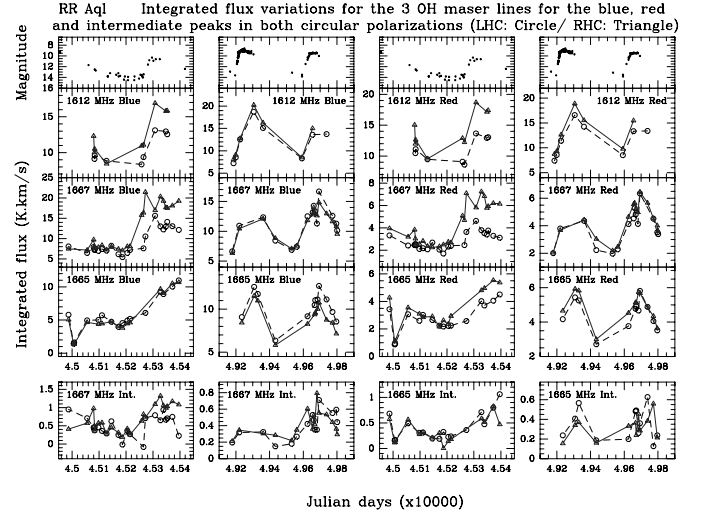
Fig. 27. Integrated flux variation curves of **RR Aql** in the 3 OH maser lines in both circular polarizations from January 1982 to March 1983 and from July 1993 to April 1995 for the blue, red and intermediate (Int.) peaks

Table 22. |[RHC−LHC]| ≥ 0.10 for the components of great longevity of **R LMi**

Freq. (MHz)	peak	$V_{\mathrm{comp.}}$ (km s^{-1})	interval *	cycle b	[RHC−LHC]
1667	blue & red	all comp.	1		from 0.24 to 0.42
	blue	-3.95	2	from (1) to (5)	0.45 ↘ 0.13
	blue	-2.50	2	from (1) to (3)	0.34 ↘ 0
	blue	-2.50	2	(5)	-0.28
	red	$+5.00$	2	from (1) to (5)	down to -0.14
	red	$+3.85$	2	from (1) to (5)	from 0.12 to 0.22
1665	blue	-4.05	1		0.16
	blue	-3.90	2	from (2) to (5)	0.66 ↘ 0.54
	blue	-3.30	1		0.59
	blue	-2.30	1		0.70
	red	$+5.00$	1		0.10
	red	$+3.45$	1		0.19

*: Same intervals as given Table 18.
b: Labelled from (1) to (5) in the second interval (cf. Fig. 24).

two epochs of observations. The measured delay between the OH and optical curves was found to be 70 ± 15 days (cf. Table 2).

The values of $\Delta I_{\mathrm{min-max}}$ for the 1612 MHz integrated flux are comparable for the two standard peaks and show a difference of less than 10% between the first and second set of observations. Main lines show greater values of $\Delta I_{\mathrm{min-max}}$ than the 1612 MHz line but difference between red and blue peak values for a given cycle are very small (<10%). On the other hand, the differences between the $\Delta I_{\mathrm{min-max}}$ of the standard peak and the inter−peak integrated flux reaches more than 30% (cf. Table 26).

As concerns its polarization, this star is quite similar to RS Vir in the sense that the 1612 and 1667 MHz emission behave similarly. Generally, temporal variations in the degree of polarization can be observed in the 3 maser lines.

Table 23. Central velocity and full width at half-maximum (FWHM) of the fitted components which have shown a longevity greater than 1 stellar period of **RR Aql** at 1612 MHz for the 2 intervals of observations. For comparison are given too in the last column the velocity of the components determined by Herman & Habing (1985, i.e., column labelled H&H)

a) Red peak

	LHC km s^{-1}	FWHM km s^{-1}	RHC km s^{-1}	FWHM km s^{-1}	H&H km s^{-1}
Interval 1[1]	$V_1 = 34.09$	0.856	$V_1 = 34.10$	0.806	34.14
	$V_2 = 32.64$	0.974	$V_2 = 32.63$	0.975	32.70
Interval 2[2]	$V_1 = 34.21$	0.738	$V_1 = 34.21$	0.746	
	$V_2 = 32.73$	0.961	$V_2 = 32.71$	0.974	

b) Blue peak

	LHC km s^{-1}	FWHM km s^{-1}	RHC km s^{-1}	FWHM km s^{-1}	H&H km s^{-1}
Interval 1[1]	$V_1 = 23.92$	0.739	$V_1 = 23.79$	0.908	
	$V_2 = 22.81$	1.066	$V_2 = 22.79$	1.034	22.85
	$V_3 = 21.33$	1.280	$V_3 = 21.34$	1.155	21.18
Interval 2[2]	$V_1 = 23.92$	0.720/0.942[(!)]	$V_1 = 24.03$	0.524	
	$V_2 = 22.82$	1.123	$V_2 = 22.86$	1.113	
	$V_3 = 21.25$	0.916	$V_3 = 21.30$	1.039	

1: Interval of Julian days [45000 − 45400].
2: Interval of Julian days [49150 − 49800].
(!): The first mean value of the FWHM given here doesn't take into account the values of the FWHM guessed as unsatisfying ones (i.e., when they are clearly greater than the whole measured FWHM over the period of observations).

Thus, a right-handed polarization observed at 1612 and 1667 MHz for the red and blue peaks as well as for the red peak at 1665 MHz in the first data set is no longer observed in the second set (cf. Table 27). The intermediate peak, observed in the main lines, shows a very small degree of polarization only at 1665 MHz for the first cycle of the second set of observations.

4.5.3. Spectral components

Figures 28–31 display the intensity variations of the fitted spectral components in the 3 maser lines for the two sets of observations which have a lifetime of a least one stellar cycle. The number of such components is less at 1612 MHz for all peaks (only 3 in the blue peak and 2 in the red one). On the other hand, both main line spectra display a highly complex profile (cf. Fig. 6) where 4 components with lifetimes greater than one stellar period in each of the standard peaks at 1665 MHz while 6 and 9 of them can be observed in the 1667 MHz red and blue peaks respectively.

Here again, all the components at 1612 MHz are very stable, they can be observed in both sets of data over more than 10 years. At 1667 MHz, only 3 of the 7 components

Table 24. Central velocity and full width at half-maximum (FWHM) of the fitted components which have shown a longevity greater than 1 stellar period of **RR Aql** at 1667 MHz for the 2 intervals of observations

a) Red and intermediate (int.) peaks

	LHC km s^{-1}	FWHM km s^{-1}	RHC km s^{-1}	FWHM km s^{-1}
Interval 1[1]	$V_1 = 33.85$	0.671	$V_1 = 33.89$	0.738
	$V_2 = 32.84$	0.649	$V_2 = 32.87$	0.695
	$V_3 = 32.08$	0.735	$V_3 = 32.11$	0.644
	$V_4 = 31.45$	0.710	$V_4 = 31.52$	0.667
	$V_5 = 30.54$	0.776	$V_5 = 30.57$	0.893
	$V_{\text{int.}} = 29.02$	0.925	$V_{\text{int.}} = 29.00$	0.864
Interval 2[2]	$V_1 = 34.07$	0.458	$V_1 = 34.08$	0.476
	$V_2 = 33.57$	0.498	$V_2 = 33.54$	0.549
	$V_3 = 32.92$	0.561	$V_3 = 32.91$	0.548
	$V_4 = 32.31$	0.653	$V_4 = 32.27$	0.729
	$V_5 = 31.57$	0.775	$V_5 = 31.58$	0.710
	$V_6 = 30.59$	0.737	$V_6 = 30.61$	0.739
	$V_{\text{int.}} = 29.02$	0.915	$V_{\text{int.}} = 28.93$	0.754

b) Blue peak

	LHC km s^{-1}	FWHM km s^{-1}	RHC km s^{-1}	FWHM km s^{-1}
Interval 1[1]	$V_1 = 27.87$	0.512	$V_1 = 27.73$	0.501
	$V_2 = 27.18$	0.636	$V_2 = 27.00$	0.692
	$V_3 = 26.25$	0.764	$V_3 = 26.19$	0.792
	$V_4 = 25.19$	0.732	$V_4 = 24.98$	0.881
	$V_5 = 24.21$	0.764	$V_5 = 24.11$	0.681
	$V_6 = 23.43$	0.952	$V_6 = 23.45$	0.785
	$V_7 = 21.89$	0.810	$V_7 = 21.96$	0.833
Interval 2[2]	$V_1 = 27.86$	0.408	$V_1 = 27.62$	0.444
	$V_2 = 27.20$	0.628	$V_2 = 27.05$	0.494
	$V_3 = 26.47$	0.553	$V_3 = 26.44$	0.468
	$V_4 = 25.71$	0.593	$V_4 = 25.78$	0.622
	$V_5 = 25.07$	0.542	$V_5 = 24.95$	0.602
	$V_6 = 24.21$	0.802	$V_6 = 24.14$	0.764
	$V_7 = 23.42$	0.515	$V_7 = 23.42$	0.504
	$V_8 = 22.98$	0.678	$V_8 = 22.93$	0.623
	$V_9 = 21.94$	0.731	$V_9 = 22.00$	0.790

1 and 2: The same intervals as given in the previous table.

observed in the red and intermediate peaks have a lifetime greater than 10 years. These components are located at a velocity of $V = 31.50$, 30.55 and $V = 29.00$ km s^{-1}. Likewise, only 5 of the 9 components observed in the 1667 MHz blue peak can be seen over more than 10 years. Those are centered at $V = 27.80$, 27.10, 24.15, 23.43 and 21.95 km s^{-1}. At 1665 MHz, changes in the spectral components are of the same order: two components are observed without ambiguity over the two sets of observations in the blue peak (at $V = 24.15$ and 27.16 km s^{-1}) against 4 in the red peak (i.e., the 4 components displayed in Fig. 29). Table 28 gives the range and mean values of $\Delta I_{\text{min}-\text{max}}$ in the three OH lines for the two intervals of observations. At 1667 MHz, the difference in amplitude of variations for a given component of the blue peak from the first data set to the second is about $15 - 20\%$ except for the component belonging to the most external part of the peak (i.e., $V = +21.95$ km s^{-1}) which shows

Table 25. Source: **RR Aql**. The same as for the previous table but for the 1665 MHz

a) Red and intermediate (int.) peaks

	LHC km s^{-1}	FWHM km s^{-1}	RHC km s^{-1}	FWHM km s^{-1}
Interval 1[1]	$V_1 = 33.48$	0.678	$V_1 = 33.42$	0.698
	$V_2 = 32.60$	0.716	$V_2 = 32.45$	0.784
	$V_3 = 31.87$	0.839	$V_3 = 31.65$	0.789
	$V_4 = 30.64$	0.906	$V_4 = 30.57$	0.841
	$V_{\text{int.}} = 29.15$	0.778	$V_{\text{int.}} = 29.09$	0.651
Interval 2[2]	$V_1 = 33.57$	0.689	$V_1 = 33.57$	0.691
	$V_2 = 32.67$	0.757	$V_2 = 32.55$	0.883
	$V_3 = 31.85$	0.902	$V_3 = 31.75$	0.774
	$V_4 = 30.58$	0.657	$V_4 = 30.69$	0.834
	$V_{\text{int.}} = 29.01$	0.622	$V_{\text{int.}} = 28.67$	0.656

b) Blue peak

	LHC km s^{-1}	FWHM km s^{-1}	RHC km s^{-1}	FWHM km s^{-1}
Interval 1[1]	$V_1 = 27.93$	0.535		
	$V_2 = 27.22$	0.580	$V_2 = 27.16$	0.779
	$V_3 = 26.38$	0.773	$V_3 = 26.36$	0.736
	$V_4 = 25.28$	0.737	$V_4 = 25.26$	0.854
	$V_5 = 24.22$	0.785	$V_5 = 24.15$	0.910
Interval 2[2]	$V_1 = 27.63$	0.378		
	$V_2 = 27.12$	0.453	$V_2 = 27.13$	0.830
	$V_3 = 26.51$	0.561	$V_3 = 26.09$	0.850
	$V_4 = 25.41$	0.936	$V_4 = 25.04$	0.886
	$V_5 = 24.33$	0.722	$V_5 = 24.16$	0.963
	$V_6 = 23.63$	0.814		

1 and 2: The same intervals as given in Table 23.

Table 26. $\Delta I_{\min-\max}$ for the integrated flux of **RR Aql**

| Frequency (MHz)	peak	$\Delta I_{\min-\max}$ interval 1[1]	interval 2[2] (1)	(2)
1612	blue	33%	43%	
	red	32%	37%	
1667	blue	49%	30%	42%
	red	53%	37%	53%
	intermediate	75%	65%	
1665	blue	60%	33%	
	red	53%	36%	
	intermediate	70%	51%	66%

1: Interval of Julian days $[45000 - 45400]$.
2: Interval of Julian days $[49150 - 49800]$ covering 2 cycles labelled (1) and (2).

Table 27. Greatest [RHC−LHC] observed in the standard peak integrated flux of **RR Aql** in the three OH lines.

Frequency (MHz)	peak	[RHC−LHC] interval 1*	interval 2*
1612		+0.21	<+0.08
1667		+0.33	≃+0.0
1665	blue		≃−0.08
	red	+0.17	<+0.10

*: The same intervals as given in the previous table.
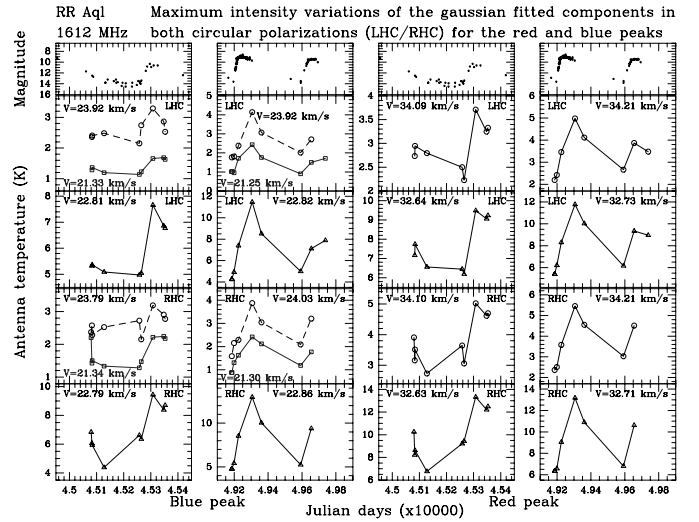
Fig. 28. Intensity variation curves of the Gaussian fitted components of **RR Aql** at 1612 MHz in left- (LHC) and right-handed (RHC) polarizations for the two standard peaks for the two sets of observations (i.e., from January 1982 to March 1983 and July 1993 to April 1995)
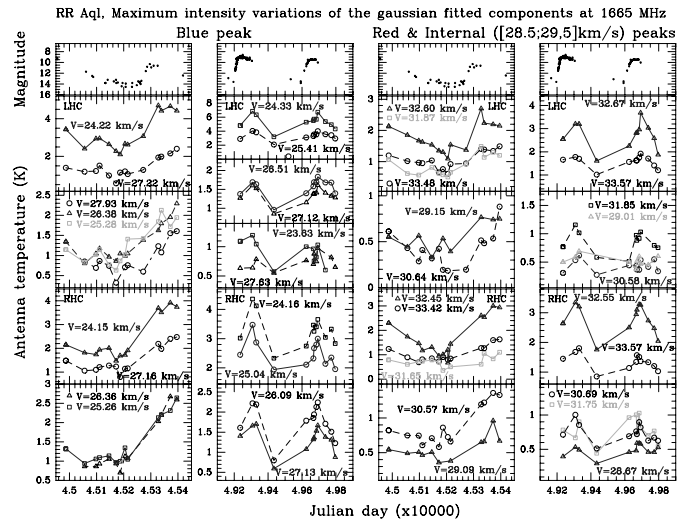

Fig. 29. Intensity variation curves of the Gaussian fitted components of **RR Aql** at 1665 MHz in left- (LHC) and right-handed (RHC) polarizations for the two standard peaks as well as for the intermediate one (components centered in the velocity interval $[+28.50; +29.50]$ km s^{-1}), for the two sets of observations (i.e., from January 1982 to March 1983 and July 1993 to April 1995)

a difference in the amplitude of variations of more than 30% between the first and the second data set.

$|[\text{RHC}-\text{LHC}]| \geq 0.10$ for the components of great longevity of RR Aql are given in Table 29. At 1612 MHz, both components of the red peak contribute equally to the observed right-handed polarization in the first set of observations. Nevertheless, the long-term components of the blue peak never reached a degree of polarization greater than 0.15 in the first data set (cf. Table 29) leading to
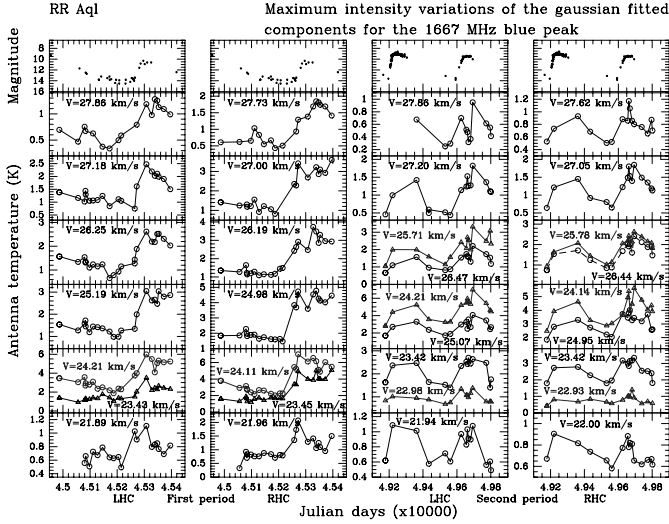
Fig. 30. Intensity variation curves of the Gaussian fitted components of **RR Aql** at 1667 MHz in left- (LHC) and right-handed (RHC) polarizations for the blue peak for the 2 sets of observations (i.e., from January 1982 to March 1983: Cols. 1 and 2 and from July 1993 to April 1995: Cols. 3 and 4)
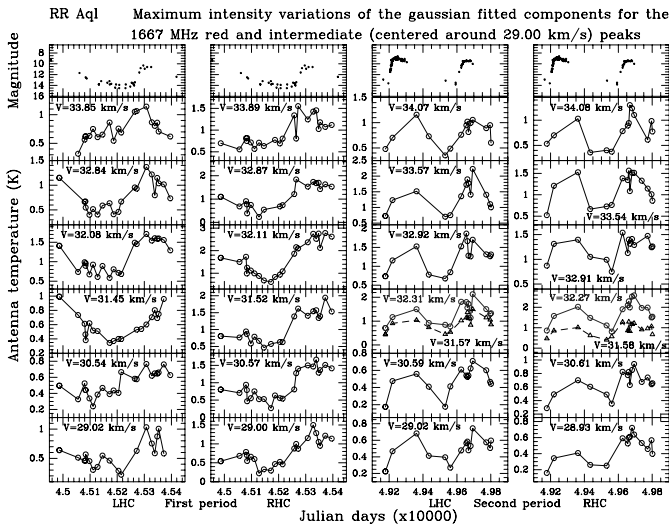
Fig. 31. Source: **RR Aql**. The same as for the previous figure but for the red and intermediate peaks, this latest being centered at $V = 29.00$ km s^{-1}

the conclusion that the right-handed polarization observed in the integrated flux of this peak is mainly due to transient components.

At 1665 MHz, the greater part of the components show a weak right-handed polarization of less than 10%, except those given in Table 29. The inter-peak component of great longevity lying in the velocity interval $[+28.5; +29.5]$ km s^{-1} shows a degree of polarization fainter than 0.10. In the first data set at 1667 MHz, the inter−peak component shows a degree of right-handed polarization of the same order as observed for the greater part of the blue peak components. On the other hand, it shows a strong degree of left-handed polarization

Table 28. Range and mean value of $\Delta I_{\mathrm{min-max}}$ for the components of great longevity of **RR Aql**

Freq. (MHz)	Peak	$\Delta I_{\mathrm{min-max}}$			
		Range		Mean Value	
		interval 1*	interval 2*	interval 1	interval 2
1612	blue	16 to 37%	40 to 47%	23%	44%
	red	21 to 30%	35 to 40%	25%	38%
1665	blue	38 ↗ 62[1]	28 ↗ 35%[2]	51%	32%
	red	35 to 64%	30 ↗ 40%[2]	47%	35%
	inter.			33%	39%
1667	blue	33 to 73%	24 to 58%	56%	40%
	red	44 to 77%	34 to 60%	60%	50%
	inter.			74%	48%

∗: The same intervals as given Table 26.
1: Rougthly increasing with the decrease of $|V_{\mathrm{component}} - V_{\mathrm{star}}|$ (i.e., $\Delta I_{\mathrm{min-max}}$ ↗ from the component centered at $V = 24.20$ km s^{-1} to the one located at $V = 27.20$ km s^{-1}).
2: Increasing with the increase of $|V_{\mathrm{component}} - V_{\mathrm{star}}|$.

Table 29. $|[\mathrm{RHC} - \mathrm{LHC}]| \geq 0.10$ for the components of great longevity of **RR Aql**

| Freq. (MHz)	peak	$V_{\mathrm{comp.}}$ (km s^{-1})	interval *	[RHC−LHC]
1612	red	21.34	1	0.14
1667	blue	all comp.	1	0.18
	blue	all comp.	2	≤ 0.12
	red	all comp.	1	0.15 ↗ 0.37[a]
	red	33.55	2	−0.22
	red	30.60	2	0.14
	inter.	29.00	1	0.19
	inter.	29.00	2[b]	−0.33
1665	blue	25.27	1	0.15
	blue	24.20	2	0.22
	red	30.60	1	0.21
	red	30.60	2	0.24

∗: The same intervals as given Table 26.
a: Increasing with the decrease of $|V_{\mathrm{star}} - V_{\mathrm{component}}|$ (i.e. from the component located at $V = +33.85$ km s^{-1} to the one located at $V = +30.55$ km s^{-1}).
b: In the first cycle of this set of data which is no longer observed in the next cycle.

($[\mathrm{RHC-LHC}] = -0.33$) in the first cycle of the second data set which totally disappeared in the next cycle.

4.6. U Her

For this star, we have more than 7 consecutive, well sampled cycles in both main lines. On average, monthly observations were performed in both circular polarizations at 1667 MHz and in right-handed polarization at 1665 MHz between July 1984 and March 1993. Sparse Observations in the left-handed polarization at 1665 MHz were performed from July 1984 to August 1991 then monthly to March 1993. This type I star shows 1612 MHz emission too but this emission will not be presented here because of its peculiarity; especially, eruptive emission could be
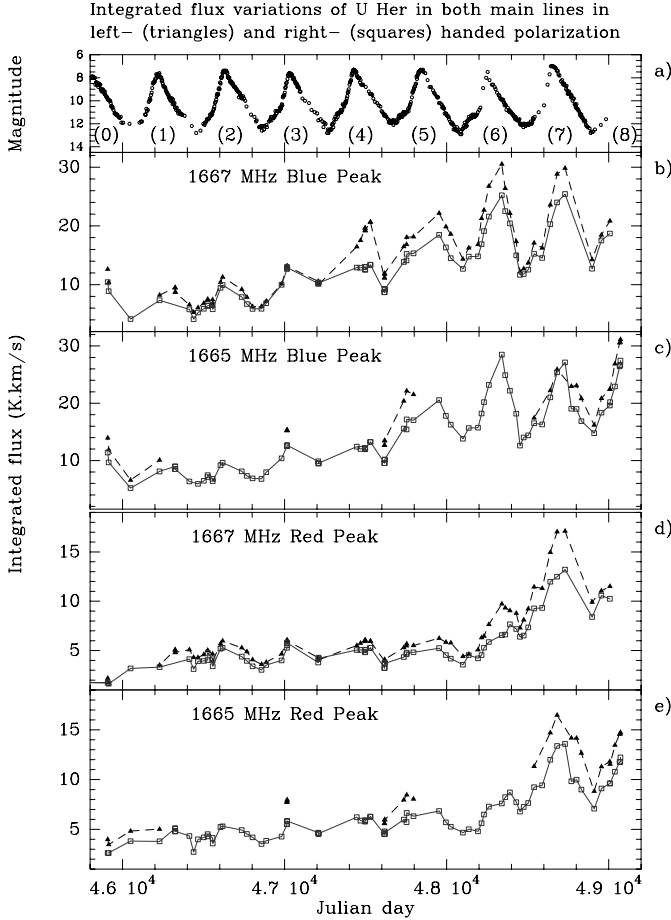
Fig. 32. Integrated flux variation curves of **U Her** in both main lines and circular polarization from July 1984 to March 1993

Table 30. Central velocity and full width at half-maximum (FWHM) of the fitted components which have shown a longevity greater than 1 stellar period of **U Her** at 1667 MHz from July 1984 to April 1993 (i.e., corresponding to [45900 − 49100] in Julian days)

a) Red peak

LHC km s^{-1}	FWHM km s^{-1}	RHC km s^{-1}	FWHM km s^{-1}
$V_1 = -8.42$	0.606	$V_1 = -8.44$	0.589
$V_2 = -9.25$	0.629	$V_2 = -9.29$	0.656
$V_3 = -9.83$	0.526	$V_3 = -9.72$	0.522
$V_4 = -10.42$	0.556	$V_4 = -10.37$	0.675
$V_5 = -10.89$	0.674	$V_5 = -10.91$	0.571
$V_6 = -11.53$	0.643	$V_6 = -11.37$	0.735
$V_7 = -12.54$	0.588	$V_7 = -12.63$	0.611

b) Blue peak

LHC km s^{-1}	FWHM km s^{-1}	RHC km s^{-1}	FWHM km s^{-1}
$V_1 = -15.15$	0.578	$V_1 = -15.20$	0.566
$V_2 = -16.08$	0.600	$V_2 = -16.02$	0.583
		$V_3 = -16.34$	0.661
$V_4 = -16.73$	0.609	$V_4 = -16.65$	0.527
$V_5 = -16.98$	0.495	$V_5 = -16.91$	0.585
$V_6 = -17.34$	0.517	$V_6 = -17.35$	0.546
$V_7 = -17.60$	0.575	$V_7 = -17.71$	0.534
$V_8 = -17.88$	0.496	$V_8 = -17.99$	0.543
$V_9 = -18.40$	0.643	$V_9 = -18.70$	0.721
$V_{10} = -18.96$	0.585	$V_{10} = -19.02$	0.603
$V_{11} = -19.38$	0.587	$V_{11} = -19.41$	0.593
$V_{12} = -19.62$	0.592	$V_{12} = -19.73$	0.621
$V_{13} = -20.11$	0.773	$V_{13} = -20.11$	0.717
$V_{14} = -20.33$	0.766	$V_{14} = -20.37$	0.738

observed from April 1984 to September 1989 as already reported by Etoka & Le Squeren (1997).

4.6.1. Spectra

Figure 7 displays the spectra of this source in both main lines and circular polarizations. One can see that the profiles and maximum intensity values are about the same in the two main lines. From the figure one can easily see that the spectral profiles are composed of many components. In both main lines, the blue peak is the widest, exhibiting 3 well defined groups of components, while the red peak is more compact. Finally, one can notice that rather strong left-handed polarization is only observed for the blue peaks at the period of the displayed observations.

4.6.2. Integrated flux

The variations of the integrated flux of U Her for the red and blue peaks in both main lines and circular polarizations are displayed in Fig. 32. The phase delay measured from the two latest, most sampled 1667 MHz cycles is about 75 days (cf. Table 2).

On the average, and considering both main lines, the integrated flux of the red peak is half that of the blue. $\Delta I_{\min-\max}$ for this star shows the smallest values observed in the main-lines ranging from 18 to 43% with a mean value of 32% for the 1667 MHz and 12 to 40% with a mean value of 25% for the 1665 MHz (cf. Table 32). Note that, the red peak integrated flux systematically exhibits fainter $\Delta I_{\min-\max}$ than the blue. Surprisingly, we notice that for this star, for a given peak the 1665 MHz integrated flux shows systematically fainter amplitudes of variations than the 1667 MHz one.

Considering each peak separately, it is clear that in trend the long-term variations of the 1667 MHz emission is very similar to that of 1665 MHz. Then, taking into consideration the general trend of the OH integrated flux variation curves, we note a rather strong increase of $\Delta I_{\min-\max}$ from cycle (5) for the blue peak and only from cycle (6) for the red peak. Furthermore, we note an increase of the mean integrated flux value (due to an increase of the minima and maxima values) along the 7.5 cycles displayed. Thus, as observed for the Mira R LMi, U Her main line emission also exhibits a long-term

Table 31. Source: **U Her**. The same as for the previous table but for the 1665 MHz

a) Red peak

LHC km s^{-1}	FWHM km s^{-1}	RHC km s^{-1}	FWHM km s^{-1}
$V_1 = -8.45$	0.523	$V_1 = -8.48$	0.490
$V_2 = -9.23$	0.560	$V_2 = -9.26$	0.552
$V_3 = -9.78$	0.470	$V_3 = -9.73$	0.429
$V_4 = -10.38$	0.670	$V_4 = -10.30$	0.660
$V_5 = -10.97$	0.780	$V_5 = -10.99$	0.530
$V_6 = -11.72$	0.637	$V_6 = -11.56$	0.612
		$V_7 = -12.75$	0.543

b) Blue peak

LHC km s^{-1}	FWHM km s^{-1}	RHC km s^{-1}	FWHM km s^{-1}
		$V_1 = -14.75$	0.447
$V_2 = -15.11$	0.642	$V_2 = -15.25$	0.596
$V_3 = -16.08$	0.675	$V_3 = -16.09$	0.632
$V_4 = -16.57$	0.609	$V_4 = -16.54$	0.587
$V_5 = -17.25$	0.752	$V_5 = -17.08$	0.721
$V_6 = -17.86$	0.532	$V_6 = -17.86$	0.603
$V_7 = -18.19$	0.655	$V_7 = -18.10$	0.560
$V_8 = -18.58$	0.668	$V_8 = -18.66$	0.696
$V_9 = -18.92$	0.620	$V_9 = -18.92$	0.655
$V_{10} = -19.43$	0.614	$V_{10} = -19.61$	0.608
$V_{11} = -20.24$	0.694	$V_{11} = -20.35$	0.685

variation of the mean integrated flux value. Note that this OH long-term variation is not correlated with the optical light curve variations.
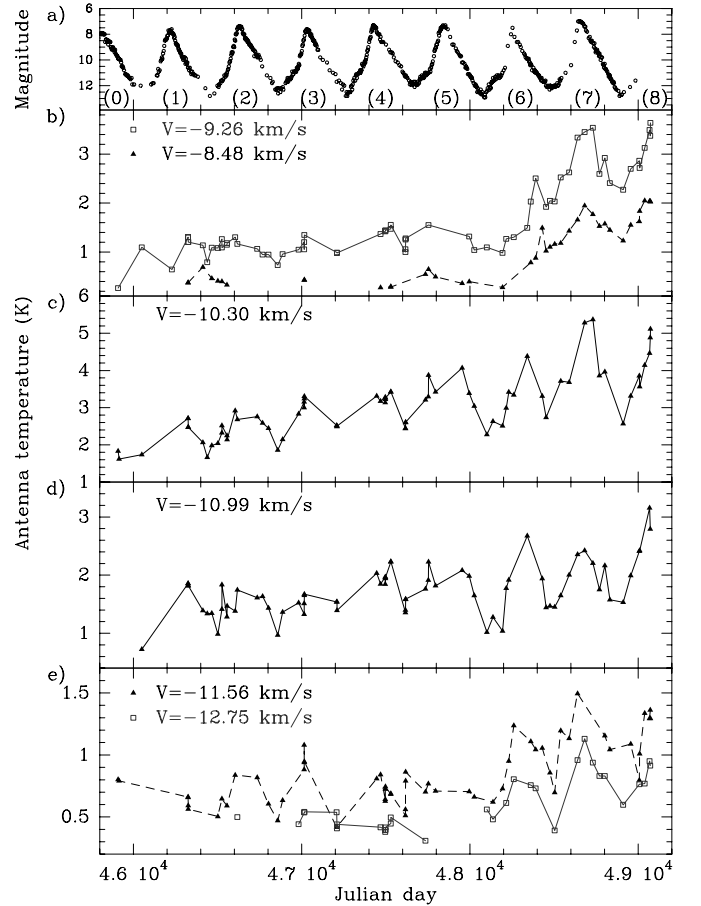
Nevertheless, a slight difference exists between the 1665 and 1667 MHz emission, especially in the degree of polarization. Few observations in the left-handed polarization at 1665 MHz were collected near the OH maximum of the cycles (0), (1), (3), (5) as well as for the entire cycle (7) and the beginning of cycle (8). They allow us to detect the presence of a faint left-handed polarization for both 1665 MHz standard peaks. The ranges of [RHC−LHC] determined at 1665 MHz for these cycles are given Table 32.

At 1667 MHz, except for cycle (3) which shows no polarization, the signal is always left-handed polarized. Nevertheless, until cycle (3) for the blue peak and cycle (5) for the red only a very faint degree of polarization was measured (cf. Table 32) after which the degree of polarization is greater. All these large values of the degree of polarization in this line occurred simultaneously with the start of the increase of the amplitude of variations. Thus, a correlation might exist between the variations in these quantities. Another interesting fact is that the left-handed polarized signal started to increase one cycle in advance of the right-handed.

4.6.3. Spectral components

Figures 33–36 display the intensity variations of the fitted components with the greatest lifetime. Because of the

Fig. 33. Intensity variation curves of the Gaussian fitted components of **U Her** at 1665 MHz in right-handed (RHC) polarization for the red peak from July 1984 to March 1993

small quantity of data in the left-handed polarization, at 1665 MHz only the variations of the components in right-handed polarization are displayed.

Spectral decomposition by Gaussian fitting reveals a great difference in behaviour between the various components, especially concerning the changes in the $\Delta I_{\mathrm{min-max}}$ from one cycle to another.
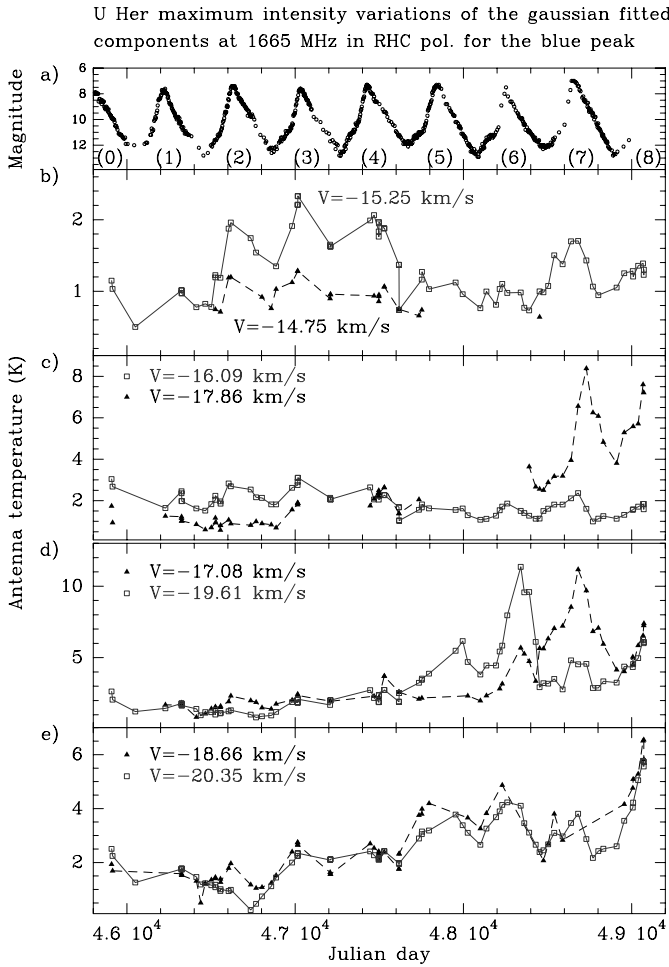
The range and mean value of the $\Delta I_{\mathrm{min-max}}$ for the components of U Her over the seven cycles are given in Table 33. At 1665 MHz, the greatest values of the amplitude of variations are attained by the most external group of components in both peaks (i.e., components located at $V = -8.48$ km s^{-1} and $V = -9.26$ km s^{-1} for the red peak and components located at $V = -19.61$ km s^{-1} and $V = -20.35$ km s^{-1} for the blue peak). The smallest amplitude values are reached by the component located at $V = -10.30$ km s^{-1} for the red peak and by the most internal component located at $V = -14.75$ km s^{-1} for the blue peak.

Table 32. $\Delta I_{\min-\max}$ and [RHC−LHC] for the integrated flux of **U Her** over the 7 consecutive cycles labelled from (1) to (7) of the interval of Julian days [45900 − 49100]

Freq. (MHz)	peak	$\Delta I_{\min-\max}$ cycles						
		(1)	(2)	(3)	(4)	(5)	(6)	(7)
1667	blue	29%	36%	36%	35%	36%	43%	42%
	red	18%	25%	26%	21%	23%	38%	40%
1665	blue	18%	25%	26%	21%	23%	38%	40%
	red	12%	20%	25%	16%	20%	30%	33%

Freq. (MHz)	peak	[RHC−LHC] cycles			
		(0)	(1)	(2)	(3)
1667	blue	< -0.10	< -0.10	< -0.10	0
	red	< -0.10	< -0.10	< -0.10	$<< -0.10$
1665	blue	$[-0.13; 0]$	$[-0.13; 0]$		$[-0.13; 0]$
	red	$[-0.15; -0.12]$	$[-0.15; -0.12]$		$[-0.15; -0.12]$

Freq. (MHz)	peak	[RHC−LHC] cycles				
		(4)	(5)	(6)	(7)	(8)
1667	blue	-0.21	$\simeq -0.10$	$\simeq -0.10$	$\simeq -0.10$	
	red	< -0.10	< -0.10	-0.19	-0.15	
1665	blue	$[-0.13; 0]$				
	red	$[-0.15; -0.12]$			-0.10	-0.10

U Her maximum intensity variations of the gaussian fitted components at 1665 MHz in RHC pol. for the blue peak

Fig. 34. Source: **U Her**. The same as for the previous figure but for the blue peak

At 1667 MHz, the mean values of $\Delta I_{\min-\max}$ are quite similar to the 1665 MHz. In the red peak, the greatest amplitudes of variations was observed for the component centered at $V = -9.83$ km s^{-1} which belongs to the most external group of components. In the blue peak, the greatest amplitudes of variations was observed for the group of components ranging in the velocity interval $[-16; -18]$ km s^{-1}.

It is clear that the increase of the mean value of the integrated flux value is due only to some specific components while other different components contribute to the changes of the amplitude of variations observed between cycles. The red peak components centered at $V = -10.30$ and -10.99 km s^{-1} at 1665 MHz are a good illustration of this fact (cf. Fig. 33). Even though they display large intensities they hardly contribute to the increase of $\Delta I_{\min-\max}$ for the integrated flux observed in cycle (7) of Fig. 32. This increase is mainly due to the components located at $V = -9.26$ and -8.48 km s^{-1} and, with less importance, components located at $V = -11.56$ and -12.75 km s^{-1}. Thus, the internal group of components of the peak (i.e., located at $V = -10.30$ and -10.99 km s^{-1}) displays a quite different and dissociated behaviour from the two external groups of components of the peak (i.e., respectively located at $V = -11.56$ and -12.75 km s^{-1} and $V = -9.26$ and -8.48 km s^{-1}).

The 1665 MHz blue peak is even more complicated since the increase of $\Delta I_{\min-\max}$ in the integrated flux from one cycle to another is due to an enhancement of intensity from different components in each cycle (cf. Fig. 34): the increase of $\Delta I_{\min-\max}$ observed in cycle (5) and (6) of Fig. 32 is mainly due to the
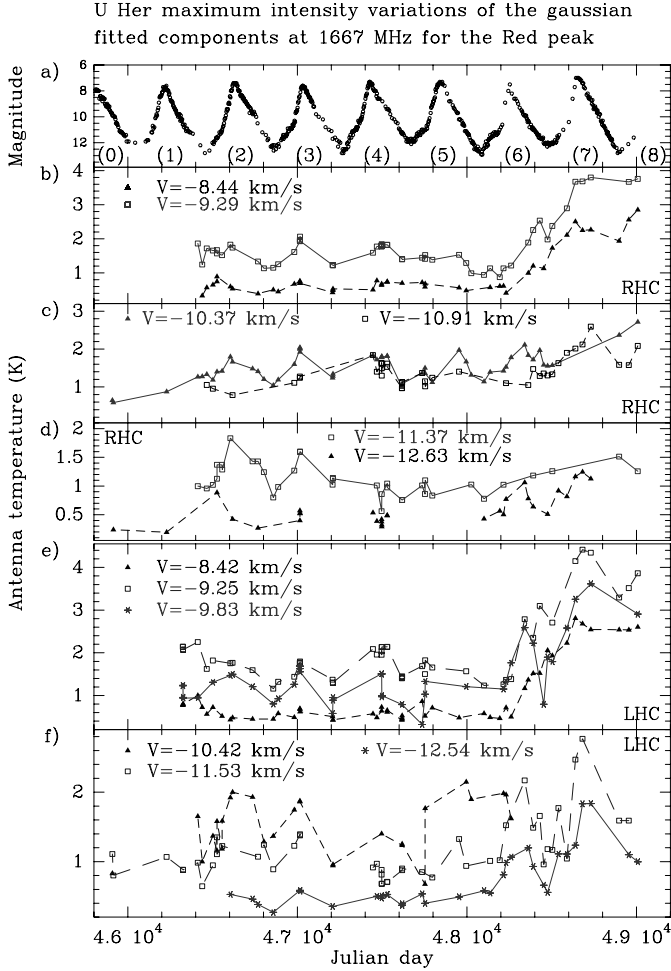
Fig. 35. Intensity variation curves of the Gaussian fitted components of **U Her** at 1667 MHz in left- (LHC) and right-handed (RHC) polarizations for the red peak from July 1984 to March 1993

Fig. 36. Source: **U Her**. The same as for the previous figure but for the blue peak

component located at $V = -19.61$ km s^{-1}, while in cycle (7) it is due to the components located at $V = -17.08$ and -17.86 km s^{-1}. On the other hand, the increase of the mean value of the integrated flux is only due to the two components located respectively at $V = -18.66$ and -20.35 km s^{-1}. The components centered at a velocity closest to the stellar velocity (i.e., at $V = -15.25$ and -14.75 km s^{-1}), show a very erratic behaviour. Moreover, a faint but continuous decrease of the mean value of the intensity of the component centered at $V = -16.09$ km s^{-1} is seen. We note that this last component is located at a velocity which is within 0.4 km s^{-1} of the 1612 MHz eruptive peak studied by Etoka & Le Squeren (1997).

At 1667 MHz, the increase of the integrated flux $\Delta I_{\mathrm{min-max}}$ in the red peak Fig. 32 is also due to the most internal group of components and located at the same velocity as in the 1665 MHz emission, i.e., at $V = -8.44$ and -9.29 km s^{-1}. The component centered at
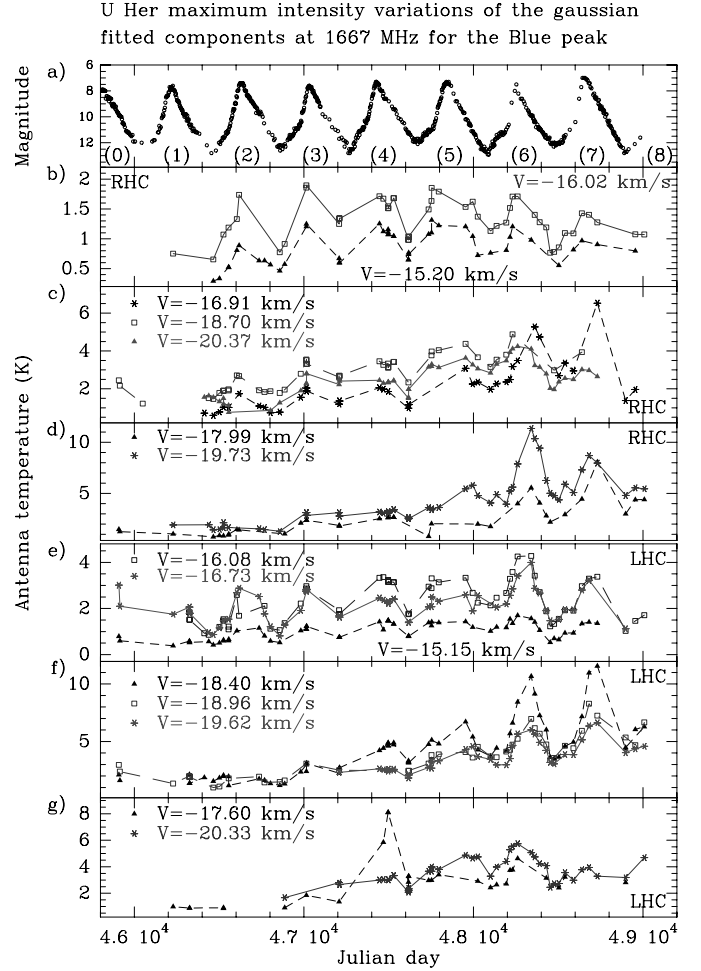
$V = -9.83$ km s^{-1} as well as the components located at $V = -12.54$ and -11.53 km s^{-1} also contribute to this amplitude increase. Here again, but with less strength, the components centered at $V = -10.37$ and -10.91 km s^{-1} show a slow but continuous increase of the mean value of their integrated flux. Thus, the 1667 MHz red peak emission shows roughly the same behaviour as the one at 1665 MHz.

Most of the 1667 MHz blue peak components show quite smooth long-term variations. Thus, main contributors to $\Delta I_{\mathrm{min-max}}$ observed in the integrated flux in Fig. 32 for this specific peak are components located at $V = -19.70$, -18.40 and -16.91 km s^{-1} in a continuous process from cycle (5) to cycle (7).

Finally, considering all the cycles, the 1667 MHz red peak components of great longevity show a degree of polarization smaller than 10% expect for the component located at $V = -10.40$ km s^{-1}, for which a left-handed polarization was observed ([RHC−LHC] = -0.14 during cycle (4)) and for the component located at $V = -12.60$ km s^{-1} for which a right-handed polarization

was observed during cycle (7) with [RHC−LHC] = 0.19. On the other hand, most of the blue peak components of great longevity show a left-handed polarization. [RHC−LHC] = −0.40 was reached for the component located at $V = -16.05$ km s^{-1} during cycle (6) and (7). Right-handed polarization was observed for the component located at $V = -19.70$ km s^{-1} (i.e., belonging to the most external group of components) from cycle (5) to (7) reaching a value as high as 30% during cycle (6), while the very most external component belonging to the same group showed a left-handed polarization of about 15% from cycle (4) to (7).

### 4.6.4. Comparison with existing maps in both main lines

Sivagnanam et al. (1990) obtained a VLA map of U Her in both main lines in left-handed polarization in March 1987. They detected compact components spread in 10 spots. Taking into account their channel separation of 0.47 km s^{-1}, the correspondence between their detected components and our spectral composition is excellent.

For four of the components detected by Sivagnanam et al. (1990) at 1665 MHz we have long term variations. These components, centered at $V = -10.3, -11.2, -14.9$ and -16.3 km s^{-1} in their maps, correspond, within less than 0.21 km s^{-1}, to our spectral components centered at $V = -10.30$ km s^{-1} and $V = -10.99$ km s^{-1} in the red peak and at $V = -14.75$ km s^{-1} and $V = -16.09$ km s^{-1} in the blue peak (cf. Figs. 33 and 34). These components, belonging to seven distinctive regions (labelled $1 - 6$ and 8 by the authors) show a smooth variation along cycles.

At 1667 MHz, we have long term variations for four of the detected components located in their maps at $V = -16.3, -16.8, -19.6$ and -20.1 km s^{-1} (corresponding, within less than 0.25 km s^{-1}, to our fitted components respectively centered at $V = -16.08, -16.73, -19.62$ and -20.33 km s^{-1}, cf. Figs. 36). These components, covering three regions in their maps (labelled 5, 9 and 10), also show smooth variations within cycles.

Chapman et al. (1994) carried out interferometric observations of U Her in both main lines in July 1984 with MERLIN. For the same field of view their distribution matches the distribution from Sivagnanam et al. (1990), showing that the stability of spectral components is accompanied by a stable, temporal maser distribution in the shell.

All these facts together enable us to conclude that, for a major part of the observed regions emitting in the main lines, there exist some stable components lasting at least 3 to 10 years. The longevity of these components, added to their location stability, is consistent with a small velocity gradient ($\epsilon \simeq 0.3$) as estimated by Chapman et al. (1994).
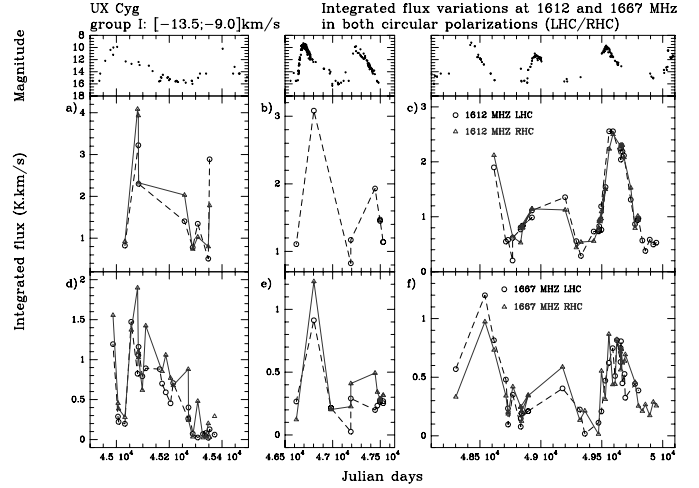

Fig. 37. Integrated flux variation curves of **UX Cyg** at 1612 **a,b,c** and 1667 MHz **d,e,f** in both circular polarizations for the group of components located at $[-13.5; -9.0]$ km s^{-1} (group I), from January 1982 to March 1983, from July 1986 to January 1989 and from February 1991 to November 1995
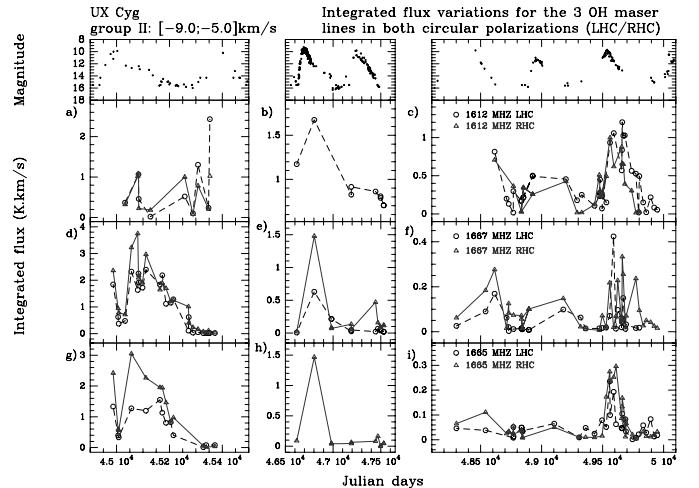
Fig. 38. Integrated flux variation curves of **UX Cyg** at 1612 **a,b,c**, 1667 **d,e,f** and 1665 MHz **g,h,i** in both circular polarizations for the group of components located at $[-9.0; -5.0]$ km s^{-1} (group II), for the 3 same intervals of time as for the previous figure

4.7. UX Cyg

This type II Mira has the largest period of the sample: about 560 days (cf. Table 1). This star was observed during 3 different epochs. The first epoch, from January 1982 to March 1983 covers 4/5 of a cycle and contains an OH maximum. The second set of data was taken with a coarser sampling between July 1986 to January 1989 but it allows us to follow the general trend of almost two cycles. The most recent set was taken from February 1991 to November 1995 over about 3 cycles in the main lines and over 2.5 cycles in the 1612 MHz satellite line. During the first and third epochs, all the observations were
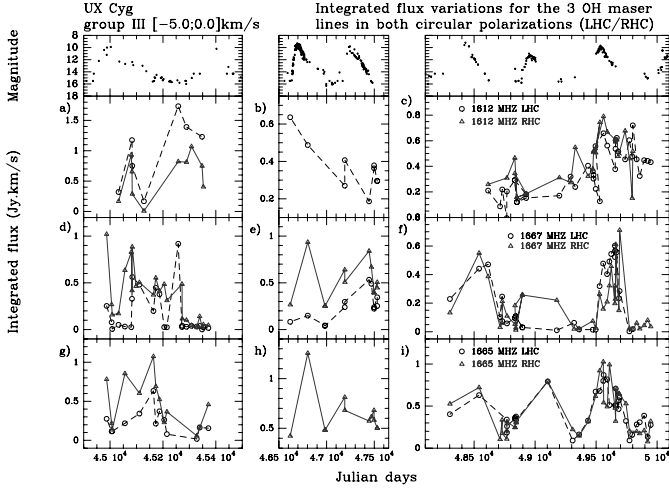
Fig. 39. Source: **UX Cyg**. The same as for the previous figure but for the group of components located at $[-5.0; 0.0]$ km s^{-1} (group III)
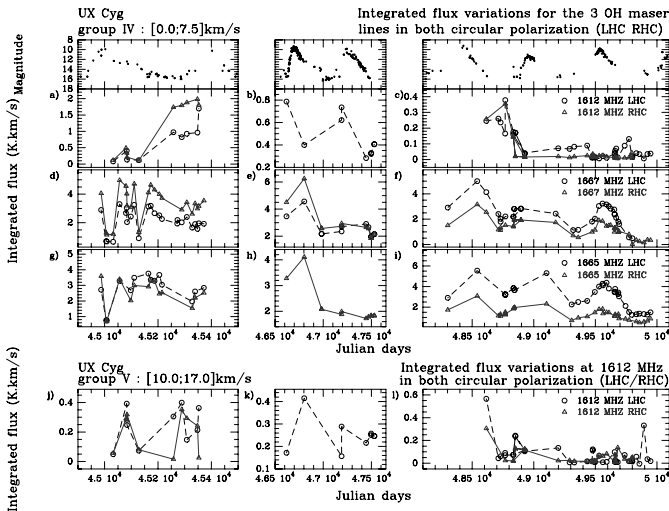
Fig. 40. Source: **UX Cyg**. The same as for the previous figure but for the group of components located at $[0.0; +7.5]$ km s^{-1} (group IV) and the one located at $[+10.0; +17.0]$ km s^{-1} (group V), this latter at 1612 MHz only

performed in both circular polarizations. For the second set of data, only the 1667 MHz observations were performed in both circular polarizations. The 1612 MHz observations were recorded in left-handed polarization and those at 1665 MHz in right-handed polarization.

4.7.1. Spectra

Figure 8 displays spectra of this source in the three OH maser lines and both circular polarizations. From this figure it is clear that the spectral profile of this source is very peculiar since we can observe 5 groups of components at 1612 and 1667 MHz which spread over more than 26 km s^{-1}. This implies a large expansion velocity

Table 33. Range and mean value of the $\Delta I_{\mathrm{min-max}}$ considering the components of great longevity of **U Her** as a whole and over the seven cylces of the interval of Julian days $[45900 - 49100]$

Freq. (MHz)	peak	$\Delta I_{\mathrm{min-max}}$ Range	mean value
1667	blue	12 to 71%	38%
	red	17 to 65%	35%
1665	blue	20 to 82%	37%
	red	17 to 69%	32%

(i.e., >10 km s^{-1}), unusual for this kind of star. For simplicity, let us define group I as the group of components in the velocity range $[-13.5; -9.0]$ km s^{-1}, group II in the velocity range of $[-9.0; -5.0]$ km s^{-1}, group III in $[-5.0; 0.0]$ km s^{-1}, group IV in $[0.0; +7.5]$ km s^{-1} and group V in $[+10.0; +17.00]$ km s^{-1}. At 1665 MHz only groups II to IV can be observed.

4.7.2. Integrated flux

The integrated flux variations of each of these groups of components in the 3 OH maser lines are displayed in Figs. 37–40 for the 3 epochs of observations. At 1667 MHz, emission of group V was usually below the threshold of detection, thus, only the integrated flux variations of groups I to IV are displayed here.

On average, emission in group V is by far the lowest and has shown the smallest amplitude changes from the first set of observations to the third one. It hardly reaches 0.6 K km s^{-1} during the third epoch of observations and, in fact, was hardly above the noise level for most of the time. Emissions from groups II and III in the main lines and from groups III and IV in the 1612 MHz satellite line are also very low in the third data set. Thus, the resulting variation curves are rather chaotic. Nevertheless, it is clear that each of these 5 groups of components undergoes cyclic variations. Thus, from the variations of the group IV during the third set of observations, a slow decline of the integrated flux of this group along the three displayed cycles is clearly seen. This is reminiscent of the slow long-term variation observed in the main-line integrated fluxes of R LMi and U Her. The phase delay, measured in the last cycle of the third data set in the strong 1612 MHz group I integrated flux, is about 80 ± 10 days (cf. Table 2).

Table 37 gives the smallest and the greatest value of $\Delta I_{\mathrm{min-max}}$ observed in each line as well as the difference between the smallest and greatest value of $\Delta I_{\mathrm{min-max}}$ observed in each group and at each frequency. For this star, taking into consideration all groups, the mean values of $\Delta I_{\mathrm{min-max}}$ are similar for the satellite line and the main lines: 65%, 71% and 65% at 1612, 1667 and

Table 34. Central velocity and full width at half-maximum (FWHM) of the fitted components which have shown a longevity greater than 1 stellar period of **UX Cyg** at 1612 MHz from February 1991 to November 1995 (i.e., $[48300 - 50000]$ in Julian days)

	LHC km s^{-1}	FWHM km s^{-1}	RHC km s^{-1}	FWHM km s^{-1}
group I$^{\mathrm{I}}$	$V_1 = -10.07$	0.685	$V_1 = -9.94$	0.811
	$V_2 = -10.52$	0.974	$V_2 = -10.31$	0.748
	$V_3 = -10.98$	0.634		
	$V_4 = -11.67$	0.806	$V_4 = -11.63$	0.779
	$V_5 = -12.22$	0.540	$V_5 = -12.18$	0.637
group II$^{\mathrm{II}}$	$V_1 = -5.51$	0.648		
	$V_2 = -8.23$	0.817		
group III$^{\mathrm{III}}$	$V_1 = -2.52$	0.742	$V_1 = -2.58$	0.893
group IV$^{\mathrm{IV}}$	(*)		(*)	
group V$^{\mathrm{V}}$	(*)		(*)	

I: Velocity range $[-13.5; -9.0]$ km s^{-1}.
II: Velocity range $[-9.0, -5.0]$ km s^{-1}.
III: Velocity range $[-5.0; 0.0]$ km s^{-1}.
IV: Velocity range $[0.0; 7.5]$ km s^{-1}.
V : Velocity range $[10.0; 17.0]$ km s^{-1}.
(*): No component showing a clear cyclic variation over more than 1 stellar period.

Table 35. Source: **UX Cyg**. The same as for the previous table but for the 1667 MHz

	LHC km s^{-1}	FWHM km s^{-1}	RHC km s^{-1}	FWHM km s^{-1}
group I$^{\mathrm{I}}$	$V_1 = -11.86$	0.679	$V_1 = -11.83$	0.753
	$V_2 = -11.56$	0.684	$V_2 = -11.44$	0.831
			$V_3 = -10.68$	0.877
group II$^{\mathrm{II}}$	(*)		(*)	
group III$^{\mathrm{III}}$			$V_1 = -4.03$	1.028
group IV$^{\mathrm{IV}}$	$V_1 = 2.31$	0.784	$V_1 = 2.55$	0.748
	$V_2 = 3.14$	0.802	$V_2 = 3.08$	0.877
	$V_3 = 3.57$	0.792	$V_3 = 3.49$	0.735
	$V_4 = 3.73$	0.872	$V_4 = 3.94$	0.710
	$V_5 = 4.79$	0.843	$V_5 = 4.61$	0.593
			$V_6 = 5.28$	0.726
group V$^{\mathrm{V}}$	(*)		(*)	

Explanation of (*) and the velocity range of the so-called groups I, II, III, IV and V are given in the previous table.

Table 36. Source: **UX Cyg**. The same as for the previous table but for the 1665 MHz

	LHC km s^{-1}	FWHM km s^{-1}	RHC km s^{-1}	FWHM km s^{-1}
group I$^{\mathrm{I}}$	(*)		(*)	
group II$^{\mathrm{II}}$	(*)		(*)	
group III$^{\mathrm{III}}$	$V_1 = -4.44$	0.731	$V_1 = -4.07$	0.959
	$V_2 = -1.46$	0.541		
group IV$^{\mathrm{IV}}$	$V_1 = 1.54$	0.704		
	$V_2 = 2.35$	0.674	$V_2 = 2.46$	0.645
	$V_3 = 3.24$	0.555	$V_3 = 3.08$	0.626
	$V_4 = 3.61$	0.819	$V_4 = 3.50$	0.686
	$V_5 = 4.04$	0.572	$V_5 = 4.10$	0.701
	$V_6 = 4.94$	0.627		
	$V_7 = 5.36$	0.828	$V_7 = 5.31$	0.917
group V$^{\mathrm{V}}$	(*)		(*)	

Explanation of (*) and the velocity range of the so-called groups I, II, III, IV and V are given in Table 34.

Table 37. $\Delta I_{\mathrm{min-max}}$ for the integrated flux of **UX Cyg**

a) The greatest value of $\Delta I_{\mathrm{min-max}}$

Frequency (MHz)	Group	interval*	$\Delta I_{\mathrm{min-max}}$
1612	II	1	92%
	IV	1	90%
1667	III	3	95%
	II	2	92%
1665	II	1	96%

b) The smallest value of $\Delta I_{\mathrm{min-max}}$

Frequency (MHz)	Group	interval*	$\Delta I_{\mathrm{min-max}}$
1612	I	2	28%
	II	2	34%
1667	IV	2	42%
	II	3	45%
1665	IV	3	31%

*: Interval of Julian days 1: $[45000 - 45400]$.
   Interval of Julian days 2: $[46600 - 47550]$.
   Interval of Julian days 3: $[48300 - 50000]$.

c) The difference between the greatest and the smallest value of $\Delta I_{\mathrm{min-max}}$ for each group and frequency.

Frequency (MHz)	Group				
	I	II	III	IV	V
1612	52%	58%	45%	46%	41%
1667	28%	47%	38%	32%	
1665		58%	36%	36%	

1665 MHz respectively. The difference between the smallest and the greatest value is quite large for the three maser lines, exeeding 30% for all lines. Surprisingly, it is the greatest at 1612 MHz, leading to the conclusion that this emission is unsaturated.

Some changes can be seen in the degree of polarization in the three maser lines. Values of $|[\mathrm{RHC{-}LHC}]| \geq 0.10$ are listed in Table 38.

The 1612 MHz satellite line is the one which shows the least change. A strong degree of left-handed and right-handed polarization is observed for groups III and IV respectively during the first interval of observations.

Otherwise the signal shows very faint polarization, especially in the very last interval of observations.

In the first interval of observations, the 1667 MHz line shows significant polarization only for group IV. During the second set of observations all groups show right-handed polarization, for which the highest values are given Table 38. Finally, during the third interval of observations, groups I, II and III show faint polarization (with the exception of the 100% right-handed polarization

Table 38. |[RHC−LHC]| ≥0.10 for the integrated flux of the 5 groups of **UX Cyg**

Freq. (MHz)	Group	interval *	[RHC−LHC]
1612	III	1	−0.36
	IV	1	0.35
1667	IV	1	0.20
	I	2	0.40
	II	2	> 0.40
	III	2	0.73
	IV	2	0.16
	IV	3	−0.22, ≤ −0.19, −0.43◇
1665	II	1	0.41
	III	1	0.59
	IV	1	−0.12 ≤ [RHC−LHC]< 0
		3	−0.29, −0.39, −0.49◇

∗: The same as given in the previous table.
◇: For the three cycles of this interval.

observed in the second cycle of this interval for group III). Only group IV shows a rather strong left-handed polarization, observable during all three cycles of this interval.

At 1665 MHz, in the first set of observations, group IV exhibits a faint left-handed polarization while groups II and III show a strong right-handed polarization. For the third interval of observations, groups II and III also show similar behaviour, different from group IV. Thus, groups II and III exhibit a degree of polarization close to zero, while group IV shows, like at 1667 MHz, a strong left-handed polarization which increases from the first cycle to the third one.

Thus, in considering all the data sets, the 1665 and 1667 MHz lines exhibit a similar general trend in polarization quite different from the 1612 MHz satellite line. It should especially be noted that the behaviour of group IV during the third data set, which is identical for both main lines, shows an increase of the degree of polarization from the first to the third cycle, i.e., while the mean integrated flux value is decreasing.

4.7.3. Spectral components

Figure 41 displays the intensity variations of fitted components showing the greatest lifetime in the 3 OH maser lines and both circular polarizations for the third data set. Because of the faintness of groups I, II and III in the main lines, the fitting was quite difficult to achieve. It is certainly the least satisfactory of the study, since some components "were lost" in the noise or in the edge of nearby stronger components. As a result, the spectral decomposition for these groups in the main lines was of poor quality. Only the results for group IV are displayed in these lines. For the same reason, only the results for groups I and III are displayed at 1612 MHz.

One can see that the variations of all the displayed components follow the optical cycle according to the usual delay expected between OH and optical curves. The range
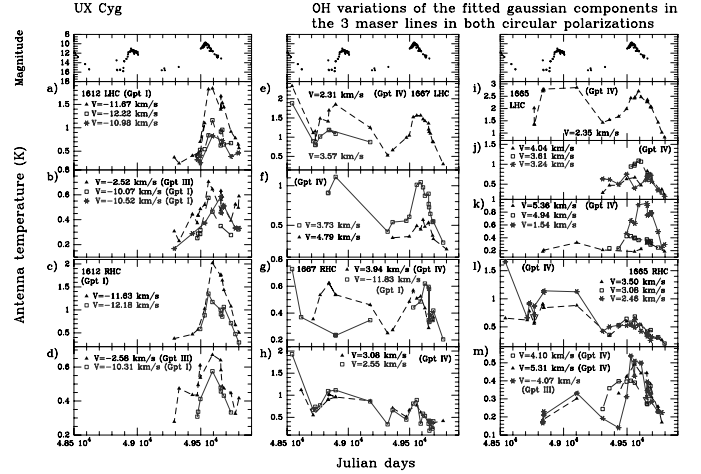
Fig. 41. Intensity variation curves of some Gaussian fitted components of **UX Cyg** in the 3 OH maser lines in left- (LHC) and right-handed (RHC) polarizations for the third set of observations (i.e., from February 1991 to November 1995). First column: 1612 MHz (i.e., boxes **a,b,c,d**), second column: 1667 MHz (i.e., boxes **e,f,g,h**) and third column: 1665 MHz (i.e., boxes **i,j,k,l,m**)

Table 39. Range and mean value of the $\Delta I_{min-max}$ considering all the components of great longevity of **UX Cyg** in the interval of Julian days [48300 − 50000]

Freq. (MHz)	$\Delta I_{min-max}$ Range	mean value
1612	30 to 70%	52%
1667	20 to 68%	48%
1665	24 to 59%	42%

and mean value of the $\Delta I_{min-max}$ considering all the components of great longevity of UX Cyg in the interval of Julian days [48300 − 50000] are given Table 39. The components at 1612 MHz exhibit the grestest values of $\Delta I_{min-max}$ while the smallest range and mean value are observed at 1665 MHz. It is clear from Fig. 41 that the variations of some of the components are rather chaotic and also for many of faint intensity.

Finally, at 1612 MHz none of the displayed fitted components exhibits a degree of polarization greater than 10%. On the other hand, at 1667 MHz, components centered at $V = 3.80$ km s^{-1} and $V = 2.40$ km s^{-1} belonging to group IV show left-handed polarization as strong as [RHC−LHC] = −0.27 while at 1665 MHz the components in the same range of velocity: at $V = 3.55$ km s^{-1} and $V = 2.40$ km s^{-1}, also show a strong left-handed polarization, as strong as [RHC−LHC] = −0.34 and −0.62 respectively. At this frequency, the component located at $V = 4.05$ km s^{-1} also shows a strong left-handed polarization with [RHC−LHC] = −0.35.

5. Discussion

In this section are presented the main characteristics of the OH flux variations over the entire sample of stars.

5.1. Comparison of the OH and optical curves

We first note that the general shape of the OH and optical variabilty curves is the same. When secondary maxima exist in the optical variability curve, they are also observed in the OH variability curves. This behaviour is well illustrated by the variability curves of the first data set (i.e., from the epoch [$45000^{\mathrm{JD}}-45400^{\mathrm{JD}}$]) of R Aql, especially, from the 1667 MHz red peak curves (cf. Figs. 9e and h in comparison with Fig. 9a). These secondary maxima can be seen in the variability curves of some components (cf. Fig. 34 cycle (7): the variability curve of the component located at $V = -17.08$ km s^{-1} of the U Her 1665 MHz blue peak).

These secondary maxima are not only observed in the OH maser emission. Indeed, they were present in H$_2$O maser emission observed by Gómez Balboa & Lépine (1986) for W Hya.

The periods determined by the fitting program show discrepancies of 1 to 20 days in comparison with those determined from the optical curves (Campbell 1985), which represents less than 6% of the period. The periods determined from the optical curves are in fact mean values determined from numerous optical cycles. Because of discrepancies between the various determinations of the optical periods, the mean optical period is reliable within 10 to 20%. The 6% deviation found between the optical and OH periods is in good agreement between the two estimations. Moreover, the estimated periods of R Aql, RR Aql and RS Vir obtained by Herman & Habing (1985) and van Langevelde et al. (1990), determined from the same rough data, are in agreement with our estimations within 10 days. On the other hand, we notice a large discrepancy between our estimations of the OH asymmetry factor and those determined by van Langevelde et al. (1990). The estimations of Herman & Habing (1985) are in better agreement with our results.

In order to determine the phase delay between the optical and OH curves as well as the OH period and the OH asymmetry factor $\Delta f_{0\,\mathrm{OH}}$ we have used the fitting program developed by David et al. (1996). We have chosen, when possible, two consecutive cycles and/or the best sampled cycle for each star. The results of the OH curve fitting are shown Fig. 42 and Table 2. In this table are given in Col. (1), the name of the sources of the study and in Cols. (2), (3) and (4) respectively, the line, polarization and peak in which the integrated flux curve fitting was performed. The period, asymmetry factor and date of the OH maximum deduced from the OH curve
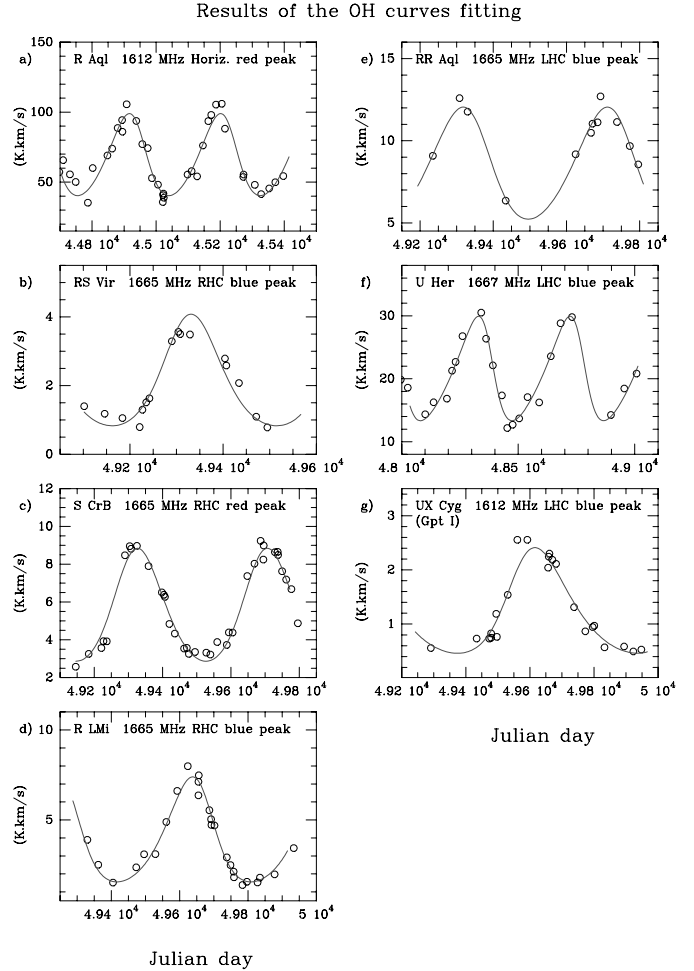
Fig. 42. Results of the fitting of the best sampled OH curve of each star

fitting are given in Cols. (5), (6) and (8). Moreover, for comparison Col. (7) gives the optical asymmetry factors obtained from the Campbell catalogue. Finally, the date of the closest optical maximum and the calculated phase delay between optical and OH maxima are given in Cols. (9) and (10).

The phase delay between the OH and the optical maximum was found to range between 10 to 20% of the period.

Even though the general shape of the OH and optical curves is the same, one still notes one peculiar difference: the asymmetry (due to a rise time from a minimum to a maximum which is different from the decline time from a maximum to a minimum) is less important in OH curves due to a smaller phase delay between optical and OH mimima than between maxima. This fact can be clearly observed from the variability curves of the S CrB main lines in the third set of observations (cf. Figs. 18f and 18g in comparison with the corresponding part of the optical light curve). Thus, if we define the asymmetry factor as:

$$f_0 = \frac{\text{ascending time from a minimum toward a maximum}}{\text{period}} \quad (2)$$

and we label the difference of asymmetry factor between OH and optical light curve

$$\Delta f_0 = f_{0\,OH} - f_{0\,optical}, \qquad (3)$$

then, except for UX Cyg which presents a very weak Δf_0 ($\Delta f_{0\,UX\,Cyg} = 0.03$) the difference of asymmetry factor is of $0.11 \leq \Delta f_0 \leq 0.25$ (cf. Table 2). This leads to the question: what kind of physical process can cause this behaviour?

The two main hypotheses which could lead to the lower value of the OH asymmetry factor are: either the number of OH molecules varies with the phase, or OH varies in phase with the infrared emission. This second hypothesis is more likely to be correct.

Maran et al. (1977), in a study of long-term infrared behaviour of Mira-type variables, note that the infrared maxima occur after the visual maxima but that no phase difference could be observed between infrared and visual minima.

The variations at 10351 Å (i.e., filter "104") as well as the variations of the composite index $D = 0.18T_1 + T_2 + V_1$ as defined by Lockwood (1972) (i.e., were T_1 and T_2 are color indexes based on TiO measurements and V_1 is an index based on VO measurements) are displayed for R Aql, S CrB, R LMi and U Her in Figs. 43a,b,c and d respectively. Also displayed in these figures is the corresponding part of the light curve (AFOEV, *private communication*). The scale of the D index and the optical curve has been changed as given in each sub-box to fit with the 104 scale, allowing a direct comparison of the locations of minima and maxima relative to the three displayed quantities. It is clear from these figures that the minima of the three curves occur at the same phase (this is clearly seen Fig. 43d for the minimum of U Her which is particularly well sampled) while the optical curves of the four stars always peak at maximum before the 104 and D curves, roughly about 0.05 phase earlier.

Moreover, from the Fig. 34 of Harvey et al. (1974), which displays the infrared observations of U Her at 1.2, 1.6, 2.2, 3.5, 4.8, 10 μm from 1968 to 1972, one can see that the optical minima indeed fit with the infrared ones while we observe a phase delay between the optical maxima and the infrared ones. It even seems that the infrared maxima are more delayed at longer wavelength in comparison with the optical maxima. Indeed, from Table A3 of Harvey et al. (1974) one see that the relative phase of the infrared maximum at 10 μm is systematically greater than the maxima at shorter infrared wavelengths 1.2, 1.6 and 2.2 μm. As the minima occur simultaneously we conclude that the asymmetry factor increases with wavelength. This leads to the conclusion that the contribution of far infrared radiation in the pumping of standard OH maser is rather strong, although the recent calculations of Collisson & Nedoluha (1993) do not confirm this.
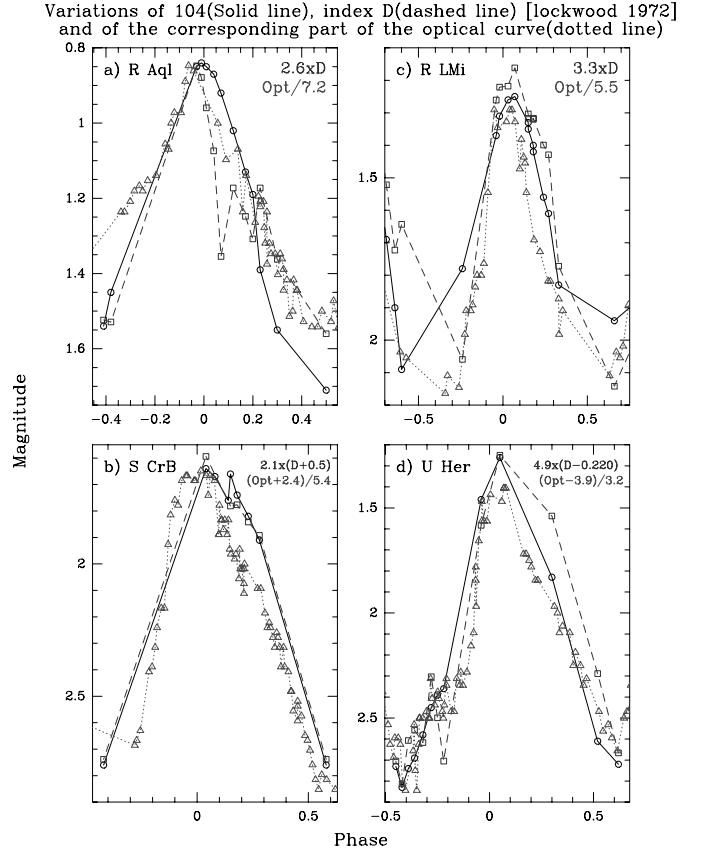
Fig. 43. Variations at 10 351 Å (i.e., filter "104") [circles with solid line] as well as the variations of the composite index $D = 0.18T_1 + T_2 + V_1$ [squares with dashed-line] defined by Lockwood (1972) were T_1 and T_2 are color indexes based on TiO measurements and V_1 is an index based on VO measurements. Also displayed is the corresponding part of the light curve (AFOEV, *private communication*) for **R Aql, S CrB, R LMi** and **U Her** [triangles with dotted line]. The scale of the D index and the optical curve have been changed as given in each sub-boxes to fit with the 104 scale allowing a direct comparison of the locations of minima and maxima of the three quantities

Finally, the OH asymmetry values given Table 2 have a mean value of $f_{0\,OH} = 0.53$. Thus, there is no systematic trend for the OH asymmetry factor to be inferior or superior to $f_{0\,OH} = 0.50$.

5.2. Polarization behaviour of the OH integrated flux

The polarization behaviour is quite different from one star to another; no evidence of a relation between the strength of the polarization and the IRAS color indexes was found (i.e., with the thickness of the dust shell). Nor was there a tendency for any of the emission to be more left or right-hand polarized. However, in all the thickest shells (i.e., R Aql, RS Vir, S CrB and UX Cyg) the general polarization trend is similar for the two main lines.

The 1612 MHz integrated flux is faintly polarized most of the time ($\leq 30\%$). On the other hand, the main lines show a degree of polarization ranging from 0 to 60%. Surprisingly, it appears that the 1667 MHz emission can be more polarized than the 1665 MHz emission (cf. integrated flux of RS Vir Fig. 12 or integrated flux of U Her in both main lines for cycle (7) in Fig. 32).

Inter−peak signal shows no or very faint polarization. For the two standard peaks, the degree of polarization is not constant. These changes differ for the front and back part of the shell, as clearly observed in R LMi. The observed changes in polarization seem to be tied to the variation of the mean integrated flux value as inferred from the main line variations of R LMi and UX Cyg. These changes seem to be tied also to the change of $\Delta I_{\min-\max}$ of the integrated flux (cf. the behaviour of U Her). Nevertheless, this link is not simple, since for R LMi the degree of polarization decreases and increases in the same manner as the mean integrated flux while for UX Cyg the behaviour is opposite.

5.3. Amplitudes of the OH integrated flux variations

Excluding UX Cyg, it appears from the measurements of the integrated flux $\Delta I_{\min-\max}$, that the 1612 MHz line always shows the smallest amplitude of variations, usually of order of $30 - 35\%$ (i.e., $I_{\max}/I_{\min} \simeq 2.0$) and hardly ever exceeding 50% (i.e., $I_{\max}/I_{\min} \simeq 3.00$). On the other hand, both main lines reach comparable values which are usually greater than 30% and can be as high as 95% (i.e., $I_{\max}/I_{\min} \simeq 40$). This fits with the idea that generally the 1612 MHz satellite line emission is considerably more saturated than the main line emissions. For all sources, changes in the amplitude of variations from one cycle to another are evident. Since the two main parameters which govern the degree of saturation are the column density of OH molecules along the line of sight and the velocity field, these changes are the signature of the dynamics of the shell physical conditions. Thus, the quick, large changes observed in the amplitude of variations in the three maser lines of UX Cyg are probably the signature of turbulence in the velocity field of its envelope. This hypothesis is strengthened by the rapidly changing shape of its spectral profile in the three maser lines.

It is striking that the 1665 and 1667 MHz emissions exhibit a similar variability behaviour different from that of 1612 MHz. Indeed, while the 1612 MHz emission usually shows small changes in amplitude it is evident that both main lines can show strong variation amplitude from one cycle to another. Moreover, close observation shows that the 1665 and 1667 MHz emissions exhibit the same variability behaviour for the same side (i.e., front or back part) of the shell. This fact is well illustrated by Fig. 32, showing the integrated flux of U Her at 1665 and 1667 MHz. Indeed, if we compare the OH variabili-

ties of the 1667 MHz red and blue peaks for example (i.e., Figs. 32b and 32d), we see that the general trend is different. We clearly observe a slow increase of the mean value of the blue 1667 MHz peak integrated flux from one cycle to another along the whole set of the displayed observations while the mean value of the red 1667 MHz peak integrated flux is constant from cycle (1) to cycle (5). Besides, the general OH variability trends, displayed in Figs. 32b and 32c (i.e., blue peaks in both main lines) and in Figs. 32d and 32e (i.e., red peaks in both main lines) are obviously similar. This fact is still valid if we compare the general 1665/67 MHz trend with the polarization as illustrated by the main line variations of R LMi Fig. 24. Indeed, we see that the blue part of the 1665 and 1667 MHz emissions show a similar behaviour, exhibiting a rather strong right-handed polarization, especially in cycles (1) and (2) (cf. Figs. 24i and 24g respectively). This behaviour is completely different from the one observed in the red part of the 1665 and 1667 MHz emissions (cf. Figs. 24j and 24h respectively) where the degree of polarization is equal to zero for the whole set of observations.

From the long term OH curves of U Her and R LMi main line integrated flux (cf. Figs. 24i, 24j and 32), we see that the temporal variation of the integrated flux mean value is not a random phenomenon but slowly varies over several cycles.

Previously, Gómez Balboa & Lépine (1986) found the existence of a super period in the H_2O maser variability curve of R Aql equal to three times the optical period. They also found a super-period in the H_2O maser emission of W Hya. As they proposed, these super-period phenomena could be the signature of shock wave effects, more precisely of an accumulation of several successive shock waves.

Recently, Bowers & Johnston (1994) have shown, from an interferometric study, that the structure of H_2O masers varies over several cycles. Also, Danchi et al. (1994) have shown, from an infrared interferometric study, that dust formation undergoes some variations over several cycles as well. Thus, it seems that two levels of variations exist in the circumstellar shell: the well known one over one period which is cyclic and a longer one which may or may not be cyclic. All these long term variations may be correlated with one another. Especially, it is obvious that variations in the dust formation will have direct consequences on the OH masers.

A theoretical study by Winters et al. (1994) has shown that emission of the circumstellar dust shell may have two components: the first which follows the cyclic periodicity of the optical light curve and a second one, spreading over several periods, which is due to the dynamical structure of the dust shell itself. Thus, all these long term variations observed in H_2O, OH and dust emission could indeed be periodic. Confirmation of this idea is important for the understanding of the pulsation mode of such stars.

Inter−peak components are only present in the profiles of the main lines. Thus, the two Miras showing such emission, i.e., RS Vir and RR Aql, do not show any inter−peak component at 1612 MHz. One can see that the red and blue peaks are well detached, with an inter−peak signal equal to zero. The only inter−peak components observed at 1612 MHz are due to eruptive emission as in U Her during 1984 and 1989 (cf. Etoka & Le Squeren 1997).

The inter−peak components do not show any special behaviour either in their OH variability or with respect to the polarization (cf. Figs. 12, 13 and 27). They all show standard OH variations and a weak degree of polarization. The faintness and the weak polarization suggest that these components may be tangential contributions from the outmost parts of the 1665−1667 MHz regions.

5.4. Component behaviour

The number of components observed in the 1612 MHz spectral profiles is generally fewer than in the main lines. Moreover, the 1612 MHz component width is smaller than that in the main lines. These two facts can be explained if the 1612 MHz emission is produced in a less turbulent zone of the envelope.

The components at 1612 MHz are stable over more than 10 years. The spectral shape at 1612 MHz shows no significant changes, while in the main lines, important changes in the number of components and in their strength occur, leading to quite different profiles from one cycle to another.

An indication of an even longer 1612 MHz velocity stability can be deduced from a comparison between the components previously detected by Herman & Habing (1985) for R Aql, RS Vir and RR Aql during the interval of Julian days [43000 − 45300] (i.e., roughly from August 1976 to November 1982) and ours. The velocity of the components detected by Herman & Habing were calculated from their Tables IIa and III where respectively are given, in Col. 7 of the first table their deduced stellar velocity and in Col. 10 of the second table the relative velocity according to the stellar one. Obviously, due to a better resolution in velocity (by about a factor 4) than the Herman & Habing study, we could detect a greater number of individual components. But, it is also clear that all the components detected by them were also detected in the present study (cf. Tables 3, 5 and 23). This then extends the stability of the 1612 MHz components to about 20 years.

All the previously mentioned facts corroborate the idea of a 1612 MHz satellite emission zone more external than the main line one.

In a general way, it is apparent from the spectral decompositions that the spectral FWHM of a single component is less than 1 km s^{-1}. Thus, a greater FWHM is due to strong blending. On the other hand, the narrowest components whose longevity is at least one stellar period have a FWHM of more than 0.3 km s^{-1}, even in spectral profiles obtained with a high spectral resolution of 0.07 km s^{-1}. According to Alcock & Ross (1986), this value corresponds to the local line width of OH molecules at 100 K. It seems that this value is a limit, independent of the spectral resolution. A very few fitted components were found to have a somehow narrower FWHM: 0.2 km s^{-1} < FWHM < 0.3 km s^{-1}. The narrowest features that Fix (1987) could distinguish from his OH spectral study of OH/IR stars at high-resolution (up to 0.014 km s^{-1}) was also 0.2 km s^{-1}. According to the model developed by Alcock & Ross (1986), Fix (1987) determined that this width corresponds to a gas temperature of about 30 K. We found that these kinds of components always have very short longevity: less than 2 months. They may be the signature of local temperature inhomogeneity. If so, we may conclude that the longevity of such local, cold blobs is no more than a few months.

Standard models, based on a uniform outflowing wind, can only create featureless profiles. However, observations at high velocity resolution clearly show that maser spectral profiles are not smooth but are in fact composed of numerous individual components. Modeling studies of Alcock & Ross (1986) have shown that these spectral profiles cannot be explained by a smooth wind. Thus, Fix (1987), from numerical modeling, has found that the actual maser profiles are consistent with emission arising from more than a thousand individual elements. In a more recent study, Zell & Fix (1990) have synthetized 1612 MHz doubly-peaked spectra of some Miras and OH/IR sources. They needed 25 individual elements to synthesize an R Aql type profile while for the other sources of their studies, they need, as did Fix (1987), about a thousand elements.

The spectral decomposition done here is such that about 10 to 20 components of about 0.3 to less than 1 km s^{-1} are needed to fit the observed spectra. Thus, considering the Zell & Fix theory, each fitted component obtained here may correspond to a whole maser blob including itself a hundred of narrow components very close in velocity (i.e., ≪ 0.2 km s^{-1}).

Bowers et al. (1989) made interferometric 1612 MHz observations of R Aql and RR Aql and 1667 MHz observations of U Her in early 1985. Some of the components they detected are the same as some of our fitted components. Especially, their OH map of U Her shows about 70% of components having the same velocity as our fitted components within our velocity resolution (0.15 km s^{-1}, which increase up to 95% within their velocity resolution of 0.30 km s^{-1}). Sivagnanam et al. (1990) and Chapman et al. (1994) also observed U Her but in both main lines. Quite good agreement of our spectral decomposition and their detected components (cf. Sect. 4.6.4) was found. All our fitted components for R Aql and RR Aql are present

(i.e., within less than 0.15 km s^{-1}) in the maps of Bowers et al. (1989). However, they detected a greater number of components for the red peak of R Aql and for both peaks of RR Aql. We attribute this discrepancy to the large FWHM of our spectral decomposition for the cited sources and peaks, especially for the blue peak components of RR Aql, which exhibit mean FWHM greater than 1 km s^{-1}, the signature of a strong blending.

In all cases, considering that a great part of the maser blobs with a specific velocity belong to the same cloud, spectral decomposition gives a way to determine the variability of a specific blob and, with maps obtained from various epochs, it could allow us to determine the change in variability according to the location of the maser blobs in the shell at a specific moment.

All the fitted components observed over more than one stellar cycle show variations in phase with the optical light curve, taking into consideration the usual delay observed between OH and optical curves.

We often observe that the most external group of components of both standard peaks (i.e., taking the stellar velocity as a reference) exhibits the greatest values of $\Delta I_{\mathrm{min-max}}$ while, surprisingly, the most internal component shows lower amplitudes. The small variations usually observed for the most internal component emission can be explained if they arise from a region lying in the outermost part of the OH shell rather than in the inner part (i.e., if it is a tangential contribution).

Moreover, considering the evolution of the OH emission over several consecutive cycles, it is clear that the mean value of the integrated flux (due to an increase or a decrease of the maxima and minima values from one cycle to another) as well as its $\Delta I_{\mathrm{min-max}}$ is not a global phenomenon but can be very different from one component to another, even though these components belong to the same peak. As can be seen in Fig. 36, components belonging to the same group (for instance U Her components centered at $V = -16.02$ and $V = -15.20$ km s^{-1} at 1667 MHz) usually show very similar behaviour. Neverthelees, sometimes large discrepancies are observed even from components of the same group as can be seen in Fig. 34 where the U Her components at 1665 MHz located at $V = -18.66$ and -20.35 km s^{-1} exhibit a similar behaviour, clearly different from the one for the component at $V = -19.61$ km s^{-1} which belongs to the same group. Now, considering the maps obtained by Bowers et al. (1989) we can see that both the $V = -18.66$ and $V = -20.35$ km s^{-1} components (i.e., $V = -18.6$ and $V = -20.2$ km s^{-1} in their maps accounting for the velocity uncertainty) are located in the same area, different from the location of the $V = -19.61$ km s^{-1} component (i.e., their component at $V = -19.7$ km s^{-1}).

It should be noted that the difference in behaviour from one component to another was previously observed in H$_2$O maser emission by Cox & Parker (1979). They

could follow the variability behaviour of the 2 close components of W Hya, respectively centered at $V = +38.2$ and $V = +40.2$ km s^{-1} and show that the variation in amplitude observed in their 1975-1976 observations was only due to the $V = +40.2$ km s^{-1} component while the $V = +38.2$ km s^{-1} component behaved regularly.

These time variations in the mean value of the integrated flux and the amplitude of the flux variation from one cycle to the next are clearly observed in the main line emissions and are not linked with any optical fluctuation of the light curves. Thus, these variations can be interpreted as a fluctuation in the degree of saturation or as local inhomogeneities either in density or velocity of the OH or/and pumping sources themselves. These phenomena are hardly observable in the 1612 MHz satellite line because of its greater saturation.

6. Conclusion

The study of the long term behaviour of OH variability of Miras is a powerful tool in the investigation of circumstellar shells under various aspects. This study showed that:

- the optical and OH periods agree within 6%;
- the optical light curves are more strongly asymmetrical than the OH ones, although the shapes of these two variability curves are similar: if there are secondary maxima in the optical curves, they are observed in the OH curve too;
- the delay at maximum in comparison with the optical one is greater in OH than at 10 μm. Since this delay increases with the wavelength in infrared radiation, the far infrared radiation coming from the dust probably plays an important role in the pumping;
- the values of the OH integrated flux minima and maxima are not correlated with those of the optical curve;
- the values of $\Delta I_{\mathrm{min-max}}$ for the integrated flux are usually of about $30 - 35\%$ at 1612 MHz, hardly ever exceeding 50%, while the amplitudes of variations in both main lines are generally greater than 30%, sometimes reaching values as high as 95%;
- the integrated flux at 1612 MHz is clearly more saturated than that of the main lines;
- the curves of the OH integrated flux coming from the front part of the shell are similar for both main lines and are different from the variability curves coming from the back part of the shell;
- the mean value of the integrated flux undergoes a slow modulation during an interval which spreads over several cycles. This is similar to recent studies which have shown that variations over several stellar cycles occur at different levels of the circumstellar shell: in the structure of the H$_2$O masers, in the dust formation and in the dynamical structure of the dust shell;

– intermediate peaks (i.e., between the red and blue ones) are only observed in the main lines and do not exhibit particular behaviour either with respect to variability or polarization;

– the degree of polarization for the 1612 MHz standard emission is less than 0.3. Only emission from the standard main line peaks exhibits degrees of polarization as high as 0.6 while inter−peak signal shows zero or very faint polarization. It also appears that the emission at 1667 MHz can be more polarized than at 1665 MHz;

– the observed changes in polarization seem to be related to the variation of the mean integrated flux value;

– the number of components in the 1612 MHz spectral profile is generally less than the number observed in the main lines, moreover the components at 1612 MHz are narrower and exhibit greater longevity;

– the components exhibit cyclic variation in phase with the optical curve if we take into account the usual delay at maximum of about $10 - 20\%$ of the period. Nevertheless, the mean value of the intensity and the amplitude of variations from a cycle to another can differ notably from one group of components to another;

– the OH variations of the most internal component of both standard peaks (taking the stellar velocity as a reference in the spectrum profile), and of the inter−peak emission usually show smaller $\Delta I_{\min-\max}$ and weaker degree of polarization in comparison with the other components, leading to the hypothesis that they are generally a tangential contribution of the outermost part emitting zones of the concerned line.

Finally, the comparison of the 1612 MHz variations with the main line ones fits with the idea that the 1612 MHz emission is more saturated and comes from of a more external zone than the main lines. Moreover, the behaviour of the OH variations is quite different from one source to another. Thus, some sources show gentle variations, certainly produced by a quite homogeneous envelope, while other sources show more complicated variations which may be due to a more inhomogeneous envelope. But, as revealed by the later interferometric studies and emphasised by the present study, it is apparent that for Miras, inhomogeneous circumstellar envelopes are quite usual. Models must take into account asymmetry even to describe the outermost parts of the circumstellar shell. Thus, Kahane & Jura (1994) needed to introduce a microturbulent velocity dispersion to reproduce their observed CO spectral shapes. The spectra in OH molecule lines also show that velocity field in the envelope is not simple. Differences observed between the variability curves of the red and blue parts of the OH shell as well as the different behaviour observed for the various groups of components belonging to a same peak also clearly show that the evolution of the circumstellar shell is quite complicated and in any case symmetrical.

References

Alcock C., Ross R.R., 1986, ApJ 305, 837

Bowers P.F., Johnston K.J., 1994, ApJS 92, 189

Bowers P.F., Johnston K.J., de Vegt C., 1989, ApJ 340, 479

Campbell L., 1985, Studies of Long Period Variables

Chapman J.M., Sivagnanam P., Cohen R.J., Le Squeren A.M., 1994, MNRAS 268, 475

Cimerman M., 1979, ApJ 228, L79

Collisson A.J., Nedoluha G.E., 1993, ApJ 413, 735

Cox G.G., Parker E.A., 1979, MNRAS 186, 197

Danchi W.C., Bester M., Degiacomi C.G., Greenhill L.J., Townes C.H., 1994, AJ 107, 1469

David P., Etoka S., Le Squeren A.M., 1996, A&AS 115, 387

Etoka S., 1996, Thesis of the "Université de Paris VI"

Etoka S., Le Squeren A.M., 1996, A&A 315, 134

Etoka S., Le Squeren A.M., 1997, A&A 321, 877

Fillit R., Proust D., Lépine J.R.D., 1977, A&A 58, 281

Fix J.D., 1987, AJ 92, 433

Gómez Balboa A.M., Lépine J.R.D., 1986, A&A 159, 166

Harvey P.M., Bechis K.T., Wilson W.J., Ball J.A., 1974, ApJS 27, 331

Herman J., Habing H.J., 1985, A&AS 59, 523

Jewell P.R., Elitzur M., Webber J.C., Snyder L.E., 1979, ApJS 41, 191

Jewell P.R., Webber J.C., Snyder L.E., 1981, ApJ 249, 118

Kahane C., Jura M., 1994, A&A 290, 183

Kurkarkin B.V., Kholopov P.N., Efremov, Yu.N., et al., 1969, General Catalog of Variable Stars, 3rd ed. Moscow

van Langevelde H.J., van der Heiden R., van Schooneveld C., 1990, A&A 239, 193

van Langevelde H.J., Janssens A.M., Goss W.M., Habing H.J., Winnberg A., 1993, A&AS 101, 109

Le Bertre T., 1993, A&AS 97, 729

Lockwood G.W., 1972, ApJS 24, 375

Maran S.P., Heinsheimer T.F., Stocker T.L., et al., 1977, Infrared Phys. 17, 565

Reid M.J., Muhleman D.O., Moran J.M., Johnston K.J., Schwartz P.R., 1977, ApJ 214, 60

Sivagnanam P., Diamond P.J., Le Squeren A.M., Biraud F., 1990, A&A 229, 171

Wilson W.J., Barrett A.H., 1968, Sci 161, 778

Winters J.M., Fleischer A.J., Gauger A., Seldmayr E., 1994, A&A 290, 623

Zell P., Fix J.D., 1990, AJ 99, 314